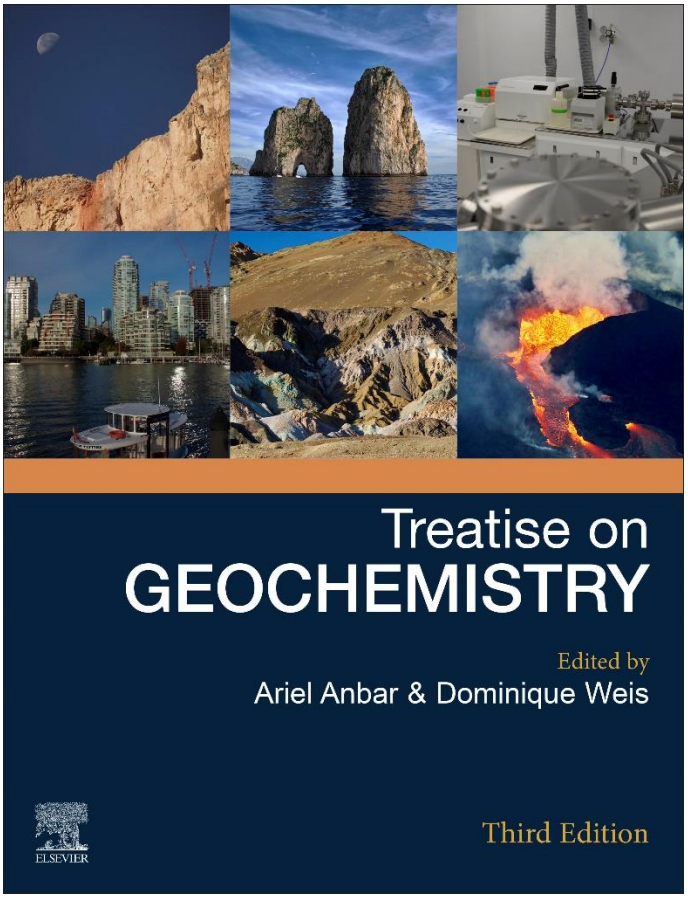

Michalski, G. (2025) Oxygen and nitrogen stable isotopes in reactive nitrogen compounds in the troposphere: A new tool for understanding tropospheric photochemistry. In: Weis, D and Anbar, A. (eds.) *Treatise on Geochemistry, 3e*. vol. 3, pp. 469-497. UK: Elsevier.

dx.doi.org/10.1016/B978-0-323-99762-1.00134-0

Oxygen and nitrogen stable isotopes in reactive nitrogen compounds in the troposphere: A new tool for understanding tropospheric photochemistry

Greg Michalski, Department of Earth, Atmospheric, and Planetary Sciences, Purdue University, West Lafayette, IN, United States; Department of Chemistry, Purdue University, West Lafayette, IN, United States

This chapter has been reviewed by the section editor Adina Paytan.

Abstract

Reactive nitrogen compounds in the troposphere plays a key role in air pollution formation (and the negative health impacts related to poor air quality), climate, acidification of rain, and the movement of key elements in biogeochemical cycles. It is therefore important to understand the sources of nitrogen oxides (NO_x), both natural and anthropogenic, and their magnitudes. Likewise, it is vital to understand the reaction pathways that oxidize NO_x into nitric acid, particulate nitrate, and other N compounds with higher oxidation states such as HONO and PAN. Stable isotope abundances have become an increasingly useful tool for both partitioning NO_x sources and probing their oxidation mechanisms. This review chapter covers recent advances in understanding variation stable isotopes abundances of NOy compounds. First, isotope abundance nomenclature for reporting variations in nitrogen and oxygen isotopes is covered, followed by and brief overview of the mechanisms that partition isotopes between reactant and products during kinetic, equilibrium, and photolysis reactions. The importance of isotope mass balance is also addressed, as is using Rayleigh distillation models to understand isotope partitioning as a function of reaction progress. The chapter then examines the observed nitrogen isotope variations in NO_x, HNO_3, NO_3^-(aq), aerosol NO_3^-, and oxygen isotope variations in important tropospheric oxidants (HOx, H_2O, O_3, O_2) as well as NO_x and NO_y compounds. Both mass dependent isotope variations and ^{17}O anomalies propagated by ozone's mass independent isotope effect are discussed. Recent experimental and theoretical research aimed at explaining the observed

isotope variation in NO_y are then examined followed by a brief review of computer modeling advances, from 0-D box models to 3-D isotope enabled chemical transport models, that try to simulate these isotope observations. The chapter concludes with some thoughts on unresolved research questions that should be addressed in future research.

Keywords

Isotope mass-dependent effects; Nitrogen; Oxygen; The Rayleigh model; Troposphere; Tropospheric oxidants; Tropospheric photochemistry

Introduction: Reactive nitrogen compounds in the troposphere

Reactive nitrogen compounds in the troposphere plays a key role in air pollution formation (and the negative health impacts related to poor air quality), climate, acidification of rain, and the movement of key elements in biogeochemical cycles. Much of reactive nitrogen is NO_x ($NO + NO_2$), which drives tropospheric oxidation chemistry, acting as a catalyst in the production of O_3 in the presence of volatile organic compounds (VOCs) (Finlayson-Pitts and Pitts, 2000; Monks, 2005). In turn, O_3 photolysis generates OH radicals that initiate a radical chain reaction in the troposphere, propagated by VOC radicals, which accelerates the oxidation of reduced compounds and thus cleanses the atmosphere (Finlayson-Pitts and Pitts, 2000; Huang et al., 2020; Kim et al., 2023; Monks, 2005). During this process, NO_x is ultimately oxidized into higher N oxides collectively known as NO_y ($NO_x + NO_3$, N_2O_5, HNO_3, $+ HNO_4 + HONO$ + Peroxyacetyl nitrates (PANs) + organic nitrates (OrgN)) as well as particulate nitrate (pNO_3^-) and NO_3^- in rain ($NO_{3(aq)}^-$) (Fig. 1). As a strong acid, atmospheric HNO_3 acidifies rain, and NO_x oxidation has become a major contributor to the acid rain problem and the acidification of aerosols (Lynch et al., 2000), which is known to have many negative environmental impacts (Brimblecombe et al., 2007). Poor air quality in urban areas, also known as SMOG (SMoke and fOG) is characterized by high levels of O_3, PAN, and particulate matter, including pNO_3^- and secondary organic aerosols produced during incomplete VOC oxidation. These compounds affect the human respiratory system, causing health problems and mortality in susceptible populations (Lighty et al., 2000) and, according to the World Health Organization, air pollution is the leading cause of environmental mortality, accounting for an estimated 7 million premature deaths annually (Lelieveld et al., 2015; Schwartz and Neas, 2000). Aerosols also have a pronounced impact on cloud physics, enhancing the absorption/reflection of solar radiation and are the largest sources of uncertainty in current climate models that predict future warming due to greenhouse gases (Chen et al., 2021; Leibensperger et al., 2012). Another important component of tropospheric reactive nitrogen is NH_3/NH_4^+, which acts primarily as a base that neutralizes tropospheric acids such as HNO_3 and H_2SO_4 (Pan et al., 2020). This neutralization can be in the gas phase with HNO_3 generating new, small particles of $NH_4NO_{3(s)}$ or in the liquid phase (cloud, fog, rain), helping to raise pH, minimizing rain acidification, and its environmental impacts. Deposition of tropospheric reactive N can occur through dry deposition of pNO_3^- (including $NH_4NO_{3(s)}$), HNO_3, NH_3, and NO_x and by wet deposition of NO_3^- and NH_4^+ via rain (rainout and washout) and fog deposition. Nitrogen deposition impacts N biogeochemistry and leads to shifts in biodiversity (Tilman et al., 1996), soil acidification (Fenn et al., 2003), poor vegetation health (Aber et al., 1998), lake eutrophication (Chapman and Edwards, 1999), and

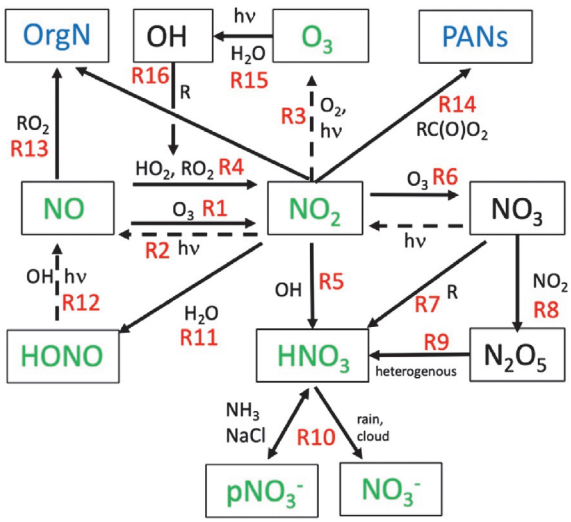

Fig. 1 The photochemical pathways (R1-16) where the primary oxidants O_3 and OH partition NO_x into various higher N oxides, collectively known as NO_y. VOCs (denoted as R) and uses NO_x as a catalyst R4, elevating O_3 above levels expected from the basic NO_x cycle (R1-3). NO_x is ultimately transformed into acids, particles, organic nitrates, and PAN that with high ozone levels defines poor air quality. Isotope effects occurring during this complex chemistry can be used to evaluate the relative importance of the photochemical oxidation pathways and help constrain NO_x sources. Compounds in green have been measured for their isotopic composition, compounds in blue will likely be analyzed in the near future.

development of coastal "dead zones" (Paerl et al., 2001; Paerl et al., 2002). Therefore, understanding sources of reactive N and photo-oxidation chemistry that transforms it into water-soluble N compounds is important for several sub-disciplines within environmental science and for understanding how this chemistry impacts society at large.

Stable isotopes of N and O have proven to be useful tools for understanding sources of N compounds emitted to the atmosphere and the photo-oxidation chemistry that converts them into highly soluble oxides that are subsequently removed from the atmosphere. This chapter presents an overview of the current state of knowledge about stable isotopes in highly reactive N compounds in the atmosphere. Isotopes in chemically, relatively stable gases, such as H_2O, CO_2, CH_4, and N_2O that are important greenhouse gases are discussed in separate chapters in this anthology. Sulfur and oxygen isotopes in SO_x cycling have recently been reviewed (Zhao et al., 2021) and will not be discussed here due to space limitations. The chapter focuses on tropospheric isotopes and not on the details of stratospheric isotope chemistry such as ozone formation via Chapman cycling. Most published isotopic measurements of reactive N compounds are of atmospheric nitrate (NO_{3atm}^-), a term that groups $HNO_{3(g)}$, $NO_3^-{}_{(aq)}$ and particulate NO_3^- (pNO_3^-) together because it is challenging to distinguish the unique forms during sampling (Michalski et al., 2003). For example, $NO_3^-{}_{(aq)}$ measured in rainwater is a combination of cloud water NO_3^- and the washout of both $HNO_{3(g)}$ and pNO_3^- in the boundary layer. Similarly, during the collection of pNO_3^- on filter paper, $HNO_{3(g)}$ can react on the substrate or aerosol accumulating on the substrate. However, recent techniques have begun to measure NO_x (Albertin et al., 2021; Walters et al., 2018), HONO (Chai and Hastings, 2018), and separated phases of NO_{3atm}^- (Blum et al., 2020) and other forms of NO_y are sure to follow. This chapter begins with a discussion of the effects that partition stable isotopes between products and reactants during photo-chemical (and biological) reactions, commonly referred to as isotope fractionation. Next is a discussion of how isotope fractionation, both chemical and biological, results in different isotope compositions of reduced N compounds emitted to the atmosphere from both natural and anthropogenic activities. A survey of direct measurements of isotope abundances in these emitted compounds is discussed in this context. This is followed by a discussion of how isotope fraction during photo-oxidation alters the initial isotopic composition of these emitted N compounds in time and space. A review of isotope measurements of the oxidized products, mainly NO_3^- is discussed in this context. This is followed by a discussion on the state of modeling stable isotope systematics, from simple 0-D photochemical box models to 3-D chemical transport models that will be invaluable for understanding isotope observations in the real world. The chapter concludes with a discussion on the research needs moving forward to maximize the use of stable isotopes in understanding reactive N compounds in not only the Earth's atmosphere but other planetary atmospheres as well.

Stable isotope abundance nomenclature, fractionations, and mass balance

During N oxidation photochemistry, naturally occurring stable isotopes of oxygen are distributed among the stable isotopes of N, forming different isotopic structures known as isotopologues and isotopomers (Alan and Andrew, 1997). An isotopologue, or isotopic homologue, is a compound with the same chemical formula and structure but with a different mass due to isotopic substitution at the same position within the molecule. For example, nitrogen dioxide has two stable nitrogen isotopologues: $^{14}NO_2$ (45.99290 amu) and $^{15}NO_2$ (46.98994 amu). Isotopomers are isotopic isomers, compounds with the same chemical formula and the same mass but a different structure due to the position of the isotopic substitution, such as ^{18}O substituted dinitrogen pentoxide (Fig. 2). Isotopomers can, but not always, have different symmetries (Fig. 2), which can play a role in mass independent isotope fractionations (see Section "Mass-independent isotope effects in photochemical systems"), and the larger the isotopologue, the larger the number of possible isotopomers.

δ and Δ notation

The isotope abundances in isotopologues are measured as ratios (R) and reported using delta notation (δ). By convention, the ratios are the less abundant isotope relative to the main isotope, e.g., $^{15}R = {}^{15}N/{}^{14}N$, $^{18}R = {}^{18}O/{}^{16}O$, and $^{17}R = {}^{17}O/{}^{16}O$. The ratios are measured with respect to internationally accepted reference materials (Coplen and Shrestha, 2016) distributed by the International Atomic Energy Agency (IAEA), the National Institute for Science and Technology (NIST, USA), or the US Geological Survey (USGS). These reference materials are, in turn, calibrated relative to a set of globally accepted reference ratios, which are air N_2 for nitrogen isotopes and standard mean ocean water (SMOW) for oxygen isotopes. The isotope delta (δ) is the difference between the measured ratio and the reference ratio, normalized to the reference ratio, and usually (but not always) scaled by 1000 and reported in parts per thousand (‰) or "per mil":

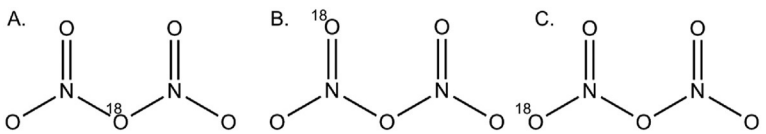

Fig. 2 Three isotopomers of the singly ^{18}O substituted dinitrogen pentoxide isotopologue (where all $N = {}^{14}N$ and $O = {}^{16}O$). The B and C isotopomers have reduced molecular symmetry (C_s) compared to the A isotopomer and unsubstituted N_2O_5 (C_{2v}). The two other isotopomers, formed by moving the ^{18}O from B or C to the right-hand side N, are degenerate with B and C and thus identical via rotation about the central O atom linking the N's.

$$\delta\ (‰) = \left(R_{sample} - R_{ref}/R_{ref}\right)1000 \quad (1)$$

Delta values can be positive or negative: In tropospheric waters, for example, the $\delta^{18}O$ averages $\sim -10‰$ relative to SMOW, while air O_2 is about +23‰. Here, and subsequently, I adopt the δ definition of $\delta^{15}NO_y = (\delta^{15}N$ value of any NO_y compound) and the same for other compounds (NH_3, O_3, etc.) and isotope deltas ($\delta^{18}O$) to minimize verbosity.

A difference between two "little deltas" are often quantified by a "big" or "CAPital" delta (Δ), where the difference can be either a measured, modeled, or theoretical difference. For example, the measured difference between the measured $\delta^{15}N$ of gaseous HNO_3 and pNO_3^-, which is sometimes called an isotope *discrimination factor*, and is denoted as $^{15}\Delta_{g\text{-}p}$ (Liu et al., 2020). When more than one isotope is in the system, Δ can be used to quantify any deviation between the measured value and the theoretical values based on the normal mass dependence of isotope partitioning (Miller, 2002). For example, there are three stable isotopes of oxygen, and the normal mass-dependent isotope effect is approximately $\delta^{17}O = 0.52 \bullet \delta^{18}O$ (see below). The $\Delta^{17}O = \delta^{17}O - 0.52 \bullet \delta^{18}O$ is then a measure of the ^{17}O excess relative to what is theoretically expected based on mass-dependent isotope fractionations. A non-zero $\Delta^{17}O$ can arise from either mass independent fractionations (MIF) or the transfer of MIF compounds to secondary compounds during photochemical reactions (see Section "Mass-independent isotope effects in photochemical systems"). The Δ has also been used to quantify the difference between a measured δ and that theoretically assuming isotope equilibrium and is thus a measure of the kinetic isotope effect in systems where both effects can play a role (Young et al., 2002). Indeed, the variations in the well-known "deuterium excess" observed in global hydrology (Gat, 1996) could be quantified using Δ notation as $\Delta D = \delta D - 8 \bullet \delta^{18}O$, where $\delta D = 8 \bullet \delta^{18}O$ is expected for water vapor in isotope equilibrium with liquid water.

Mass-dependent isotope effects in photochemical systems

During the photochemical oxidation of reduced N compounds in the atmosphere, there are differences in isotopologue rate constants leading to differences in the partitioning of isotopes between products and reactants, a process known as isotopic fractionation. These isotope fractionation effects can be classified into three well-known effects: kinetic isotope effects (KIE), equilibrium isotope effects (EIE), and vapor pressure isotope effects (VPIE). A KIE is a relative change in the rate of a unidirectional chemical reaction when one of the atoms of the reactants is substituted with an isotope (Bigeleisen and Wolfsberg, 1958). KIEs are driven mainly by differences in the two isotopologue reactants' zero-point and activation energy required to proceed through a transition state to products (Wolfsberg et al., 2010) and isotopologue differences in quantum mechanical tunneling probabilities (mainly for hydrogen isotopologues). This generally results in lighter isotopologues reacting faster than heavier ones. Much of the early research on KIEs were investigations about reactions containing hydrogen isotopes (see Kaye, 1992) and these studies usually defined a $KIE = k_L/k_H = \alpha_{L/H}$, where the k's are the rate constants for the light (L) and heavy (H) isotopologues and α is called the isotope fractionation factor that is a number that is usually very close to 1 (± 0.1). This is the inverse of the definition of α usually defined in research dealing with EIE and VPIE, and this inversion can lead to confusion. To maintain consistency between the α values for EIE, KIE, and VPIE, α will be defined here as heavy/light for all isotope effects. Gas diffusion induces a KIE, with light isotopologues unidirectionally diffusing faster than heavy ones across a concentration gradient, which may be important in atmospheric chemistry when considering the uptake of gases by atmospheric droplets (rain, cloud, or fog) or on aerosol surfaces. Urey (1947) and Bigeleisen and Mayer (1947) showed that EIEs are driven by the sensitivity of molecular vibrational frequencies to isotopic substitutions (Bigeleisen and Mayer, 1947; Urey, 1947). Since vibrations are used in molecular partition functions to calculate equilibrium constants, isotopic substitution results in isotopologues having different equilibrium constants. Analogous to the KIE, the $EIE = K_H/K_L = \alpha_{H/L}$ where the Ks are the heavy and light isotopologue equilibrium constants and $\alpha_{H/L}$ is the isotope equilibrium fractionation factor, which is temperature dependent. Isotopologues also partition differently between phases giving rise to the VPIE, which is a special case of EIE. In the VPIE, in addition to intermolecular vibrations one must account for the intramolecular vibrations that also play a role phase change equilibrium (Bigeleisen, 1961; Van Hook et al., 2001). This is most notable in gas-liquid systems and has been used extensively to understand water isotopologue fractionations in the hydrologic cycle (Gat, 1996). The VPIE may be important in reactive N compounds in the atmosphere via equilibrium between isotopologues in the gas phase and those in cloud or rain droplets such as $HNO_{3(g)} \leftrightarrow HNO_{3(aq)} \leftrightarrow H^+ + NO_3^-$. The VPIE can also occur in gas-solid equilibrium and may be relevant for reactions such as $HNO_{3(g)} + NH_{3(g)} \leftrightarrow NH_4NO_{3(s)}$, whose temperature-dependent equilibrium can shift dramatically diurnally (Morino et al., 2006) and seasonally (Paulot et al., 2016).

The α values for KIE, EIE, and VPIE can be determined either by experiment or by calculations. Experimental α values have been determined for some of the basic N reactions relevant to tropospheric chemistry (Friedman and Bigeleisen, 1950; Li et al., 2020; Walters et al., 2016). Tropospheric chemistry is, more often than not, characterized by reactions involving radicals and compounds with very low number densities making an experimental determination of α's in all but the simplest reactions a challenge. Instead, it is more common to rely on calculating α's since experimental and theoretical α values are usually close to each other within a reasonable uncertainty. These calculations require that molecular harmonic frequencies and anharmonicity constants of an isotopologue pair to be known or calculated. For KIE this requires knowing the isotopologue vibrations in the transition state, which is often approximated (Bigeleisen and Wolfsberg, 1958; Young et al., 2002) and occasionally calculated, such as the KIE for the NO + O_3 reaction (Walters and Michalski, 2016a). Urey (1947) calculated isotopologue reduced partition functions (Q's) whose

only variables are the harmonic frequencies and temperature and defined the "β value" as the ratio of two isotopologues reduced partition functions. For example, the reduced partition function ratio of nitric oxide N isotopologues is $Q_{15NO}/Q_{NO} = \beta_{NO}$, with the heavy isotope placed in the numerator by convention. The isotope exchange fractionation factor is the ratio of two β values and is denoted by $\alpha_{\beta1/\beta2}$. For example, $\alpha_{NO/NO2}$ is the temperature-dependent isotope fractionation factor for the

$$NO + {}^{15}NO_2 \leftrightarrow {}^{15}NO + NO_2 \quad \text{(EX. 1)}$$

isotope exchange reaction that has values of $\beta_{NO} = 1.0669$ and $\beta_{NO2} = 1.1064$ (at 298 K) and $\alpha_{NO/NO2} = \beta_{NO}/\beta_{NO2} = 0.9643$ (Walters and Michalski, 2015). Accurate isotopologue vibrational constants are difficult to accurately measure for large molecules, and as a result, measurements are mainly limited to diatomic and triatomic isotopologues (Richet et al., 1977). To determine the EIE in larger compounds or radicals, we must rely on quantum chemistry computation methods to estimate the molecular vibrational and anharmonicity constants. Recent works utilizing these methods have estimated the EIE for oxygen and nitrogen isotopes for most non-organic NO_y compounds (Walters and Michalski, 2015; Walters and Michalski, 2016b). Also, it is common to define an isotope enrichment factor (ε) between products (p) and reactants (r) as $\varepsilon_{p/r}$ (‰) = 1000lnα ~1000(α-1) (Criss, 1999), which expresses the fractionation factor in the same permil notation as isotope abundance differences. In the above example, the isotope enrichment factor for the NO-NO_2 isotope exchange reaction would be $\varepsilon_{NO/NO2} = -35.7$‰, which simply means at equilibrium NO would contain 35.7 parts per thousand less ^{15}N than NO_2.

A lesser-known isotope effect that is important in atmospheric systems is the photo-induced isotope fractionation effect (PHIFE). PHIFE is the relative change in the photolysis rate of an isotopologue due to the substitution of a heavier isotope (Yung and Miller, 1997; Miller and Yung, 2000) and can be estimated using a simple zero-point energy shift model (ΔZPE). In this approximation, the absorption spectra of the heavier isotopologue are generated by applying a uniform blue shift equal to the ΔZPE between the heavy and light isotopologue (Blake et al., 2003; Liang et al., 2004; Miller and Yung, 2000). This results in isotopic fractionation because the isotopologue (x) photolysis rate constant (^xJ) at any wavelength (λ) depends on the convolution of the wavelength-dependent absorption cross-section (σ(λ)), actinic flux (F(λ)), and quantum yield (ϕ(λ)) (Eq. 2):

$$j^x(\lambda) = \sigma^x(\lambda)F(\lambda)\phi(\lambda) \quad (2)$$

The overall photolysis rate constant (j^x) can be calculated by integrating σ, F, and ϕ over a range of wavelengths (λ_1 to λ_2) that can cause the isotopologue to dissociate (when $\phi \neq 0$).

$$j^x = \int_{\lambda_1}^{\lambda_2} \sigma^x(\lambda)F(\lambda)\phi(\lambda) \quad (3)$$

The N isotopologue fractionation (α) resulting from photolysis (of NO_2 isotopologues) is calculated by Eq. (4).

$$\alpha_{47/46} = \frac{j^{47}}{j^{46}} \quad (4)$$

It is important to note that there are limitations in the ΔZPE-shift model (Blake et al., 2003; Liang et al., 2004; Miller and Yung, 2000). These include the failure to account for changes in shape and intensity of absorption spectra upon isotopic substitution, and the quantum yield (as a function of wavelength) is assumed to be the same for all isotopologues. Despite these limitations, this approach should still give a rough estimate of photolytic fractionation until experimental or improved theoretical determined PHIFEs become available.

When an element has two or more stable isotopes, their δ values have a roughly linear relationship since the KIE, EIE, VPIE, or PHIFE partition between products and reactants as a function of their relative mass differences. For example, oxygen has 3 stable isotopes (^{16}O,^{17}O, and ^{18}O), and isotope effects quantified by the mass relation equations, in the harmonic approximation, are square roots of either inverse atomic mass (EIE) or reduced atomic mass (KIE) (Young et al., 2002)

$$\alpha_{\frac{17}{16}} = \left(\alpha_{\frac{18}{16}}\right)^{\beta} \quad (5)$$

$$\beta = \frac{\frac{1}{16} - \frac{1}{17}}{\frac{1}{16} - \frac{1}{18}}\ (EIE), \beta = \frac{ln\left(\frac{16}{17}\right)}{ln\left(\frac{16}{18}\right)}\ (KIE) \quad (6)$$

resulting in the linear equations $\delta^{17}O = 0.529 \bullet \delta^{18}O$ (EIE) or $\delta^{17}O = 0.515 \bullet \delta^{18}O$ (KIE). In a system where both KIE and EIE are at play, such as the troposphere, the β value is taken as 0.52 (Thiemens et al., 2001). The $\delta^{17}O$ and $\delta^{18}O$ values of many natural compounds have been measured, and the resulting array of $\delta^{17}O = 0.52 \bullet \delta^{18}O$ is often referred to as the terrestrial (isotope) fractionation line or TFL (Fig. 4).

$$\delta^{17}O = 0.52 \bullet \delta^{18}O = TFL \quad (7)$$

Mass-dependent isotope effects of N sources

The isotope mass-dependent effects (KIE, EIE, VPIE) occur not only in the atmosphere but also during the chemical and biological production of precursor gases such as NO_x. For example, when NO is produced by incomplete bacterial denitrification of NO_3^-, the microbes induce a KIE and produce ^{15}N depleted NO relative to the NO_3^- reactant (Li and Wang, 2008). Likewise, NO_x produced in internal combustion engines (ICE) tends to produce isotopically light NO_x, but this NO_x becomes progressively enriched as it is reduced by 3-way catalytic converters in the vehicle's exhaust system (Walters et al., 2015a,b). The result is that some sources of NO_x (but not all) tend to have unique $\delta^{15}N$ values depending on the KIE, EIE, or VPIE that are in play during their production (Elliott et al., 2019). This "source effect" can be important for understanding $\delta^{15}N$ variations in NO_y compounds and will be discussed in detail in Section "Isotopes of N in precursor gases NO_x and NH_3" of this chapter.

Mass-independent isotope effects in photochemical systems

Isotope effects in photochemical systems are also unique in that they also have been shown to exhibit, in rare cases, mass-independent isotope effects. When KIE, EIE, and PHIFE occur they all follow the mass-dependent isotope fractionation rule of $\delta^{17}O = 0.52\delta^{18}O$ (Eq. 7). This rule has been shown to hold true for most natural compounds in the environment, such as silicates, carbonates, waters, and O_2 that together make up the 99.999% of surface O on Earth and results in the oxygen isotope terrestrial fractionation line (TFL) in three isotope space (Fig. 4). The notable exception to the mass-dependent isotope fractionation rule (Eq. 7) is the mass-independent fractionation (MIF) that occurs during ozone formation (Heidenreich and Thiemens, 1983; Thiemens and Heidenreich, 1983). This isotope effect has been called "strange" (Gao and Marcus, 2001) because the O_3 product becomes highly enriched in the ^{18}O isotopes ($\delta^{18}O \sim 100‰$) relative to the O_2 reactant (Mauersberger et al., 1993). Further, and even stranger, the process fractionates "mass independently", i.e., both ^{17}O and ^{18}O become equally enriched, with the products and residual reactant falling on a slope 1 line in dual isotope ratio space (Thiemens and Heidenreich, 1983) This deviation between the observed and theoretically expected values is quantified precisely (Eq. 8) but more often approximately (Eq. 9) by (Miller, 2002):

$$\Delta^{17}O = 1000 \bullet \ln\left(1 + \frac{\delta^{17}O}{1000}\right) - \lambda \bullet 1000 \bullet \left(1 + \frac{\delta^{18}O}{1000}\right) \quad (8)$$

$$\Delta^{17}O = \delta^{17}O - \lambda \bullet \delta^{18}O \quad (9)$$

A mass-dependent coefficient $\lambda = 0.52$ is an observational average, while the mass-dependent process for any given reaction can range from 0.505 to over 0.53 depending on whether the system is controlled by KIE or EIE and the mass of the atom to which the isotope is bonded. But these different definitions and coefficient choices have only a minor impact on the resulting $\Delta^{17}O$ values, typically less than 1‰. This ozone effect has become known as a MIF: mass-independent fractionation (Thiemens, 2005, 2013; Thiemens et al., 2001). Here MIF has a specific meaning: Reactants, whose isotopic composition lies on the mass-dependent fractionation line, react, and generate products and residual reactants that fall off of the mass-dependent line with positive (negative) $\Delta^{17}O$ values (Fig. 4). MIF is a not fully understood chemical *process*, and to date, the only known significant known oxygen MIF reaction occurs during ozone formation.

An observed $\Delta^{17}O$ value, on the other hand, also called a ^{17}O anomaly, is simply a measure of the ^{17}O excess observed relative to that expected based on its theoretical mass-dependence relative to $\delta^{18}O$, and this excess is conveniently expressed by Eq. 9. This ^{17}O anomaly can arise from MIF, but this is rare with ozone formation being the only known chemical MIF. More common is the $\Delta^{17}O$ composition being transferred by isotope mass balance. Since ozone is a powerful oxidizer and O atoms can transfer from O_3 during oxidation reactions involving SO_x (Savarino et al., 2000), NO_x (Michalski et al., 2014), and HO_x (Savarino and Thiemens, 1999b). This generates $\Delta^{17}O$ compositions in compounds such as nitrate, sulfate, and hydrogen peroxide during experiments as well as being observed in real-world samples. Tropospheric O_3 $\Delta^{17}O$ and $\delta^{18}O$ values and those expected based on laboratory experiments will be discussed in Section "Isotopologues of tropospheric oxidants" since these values will be important for understanding the isotopic composition of NO_y. While the many theoretical attempts to understand the physics behind the ozone MIF are of great scientific interest (Gao and Marcus, 2001; Marcus, 2004), they are generally not germane to the compounds in this review, and have been reviewed elsewhere (Thiemens, 2013). There is also a MIF in sulfur isotopes generated during UV photolysis of SO_2, which has important implications for understanding the rise of oxygen on Earth. But UV photolysis of SO_2 is not an important process in the Earth's current troposphere, so this effect will not be discussed in this review (Masterson et al., 2011).

Isotope mass balance

Another important consideration for understanding isotope reaction systematics in the troposphere is maintaining material balance, also known as isotope mass balance. Isotopic fractionation processes do not produce or consume isotopes, rather they partition them between products and reactants. Thus, when considering a system in its entirety, the initial isotope abundances must be conserved. Take, for example, the $\delta^{15}N$ value of NO_x emitted into the troposphere, mainly as NO, during the daytime in the presence of O_3. It reaches a photochemical steady state via the NO_x cycle on the order of a few minutes (Fig. 1):

$$NO + O_3 \rightarrow NO_2 + O_2 \quad (R1)$$

$$NO_2 + h\nu\ (<420\ nm) \rightarrow NO + O \quad (R2)$$

$$O + O_2 + M \rightarrow O_3 + M \quad (R3)$$

Here hν are photons (with wavelengths less than 420 nm), and M is any gas acting as a collisional third body. Regardless of any isotope fractionation process occurring during R1–R3, isotope mass balance constrains the system (assuming no further oxidation) by:

$$\delta^{15}NO_x = f_{NO} \bullet \delta^{15}NO + f_{NO2} \bullet \delta^{15}NO_2 \quad (10)$$

Where f_{NO} and f_{NO2} are the NO_x mole fractions of NO and NO_2 and $\delta^{15}NO_x$, $\delta^{15}NO$, and $\delta^{15}NO_2$ are the $\delta^{15}N$ values of NO_x, NO, and NO_2, respectively. This simple system is commonly called a two-component isotope mixing model (Kendall, 1998) with two (isotopic) "endmembers" ($\delta^{15}NO$ and $\delta^{15}NO_2$). A more general form of isotope mass balance for a system having mole fractions (f) and δ values for (i) number of compounds is,

$$\delta_{total} = \Sigma f_i \bullet \delta_i \quad (11)$$

This applies to reactive N in the troposphere as emitted NO_x is further oxidized into a variety of NO_y (i) compounds.

$$\delta^{15}NO_{x\ emitted} = \Sigma f_{NOy(i)} \bullet \delta^{15}NO_{y(i)} \quad (12)$$

This assumes a closed system, where the emitted NO_x $\delta^{15}N$ value ($\delta^{15}NO_{x\ emitted}$) is constant and no NO_x is transported into or out of the system. In an urban system where the fractions of other NO_y compounds are very small relative to NO_x, HNO_3, and pNO_3^- then:

$$\delta^{15}NO_{x\ emitted} = f_{NO} \bullet \delta^{15}NO + f_{NO2} \bullet \delta^{15}NO_2 + f_{HNO3} \bullet \delta^{15}HNO_3 + f_{pNO3} \bullet \delta^{15}NO_3^{-}{}_{(p)} \quad (13)$$

Thus simultaneous $\delta^{15}N$ and concentration measurements of these 4 NO_y compounds yields the $\delta^{15}N$ value of NO_x emitted that could then be used to assess the relative contribution of various NO_x sources to the system. To date, no study has measured these four simultaneously; rather, one NO_y compound is typically measured, and the $\delta^{15}N$ value is often interpreted as a proxy for $\delta^{15}NO_{x\ emitted}$. This interpretation is tenuous for several reasons. First, the NO_y fractions are a strong function of local atmospheric conditions. For example, when local isoprene emissions are high, the NO_y fractions of organo-nitrates and PAN may be quite high and must be included in Eq. (13). Or after a rain event, the fractions of HNO_3 and pNO_3^- may be very small relative to NO_2 and NO. Secondly, the system is rarely closed; rather, tropospheric transport by advection and convection occurs at fairly rapid times scales, and thus NO_x and NO_y measured at one location may be influenced by NO_x emissions and NO_y photochemistry that occurred elsewhere.

Isotope partitioning during reaction progress: The Rayleigh model

The partitioning of isotopes between products and reactants as a function of reaction progress is also important for understanding δ variations in the troposphere and this partitioning has been modeled using the theory that describes the separation of compounds via distillation proposed by Rayleigh (Rayleigh, 1902). While the Rayleigh distillation equations formally describe equilibrium between different phases (EIE), it has also been used to describe isotope behavior in systems where KIE and PHIFE are the fractionating effects (Rahn et al., 1998). The change in δ values in the product and reactant as the reaction progresses depends on whether the system is closed or open (Kendall, 1998). Closed Rayleigh distillations occur in systems where chemical and isotopic equilibrium is always maintained between the products and reactants (or phases), and isotope mass balance is always maintained. Consider gas phase HNO_3 equilibrating with newly formed cloud droplets forming a solution of HNO_3. The delta value of HNO_3 in the gas ($\delta_{(g)}$) and liquid ($\delta_{(l)}$) phase at any point in the distillation is a function of the initial δ value of the gas ($\delta_{(g)o}$), the fraction of HNO_3 remaining in the gas phase ($f_{(g)}$), and the isotope enrichment factor of the HNO_3 in the liquid phase relative to the gas ($\varepsilon_{l/g}$):

$$\delta_{(aq)} = \delta_{(g)o} + f_{(g)} \bullet \varepsilon_{l/v} \quad (14)$$

$$\delta_{(g)} = \delta_{(g)o} - \left(1 - f_{(g)}\right) \bullet \varepsilon_{l/v} \quad (15)$$

In the HNO_3 case, due to the very high effective Henry's law constant for HNO_3 ($\sim 10^{15}$ M/atm), essentially all HNO_3 will partition into the aqueous phase on a relatively short timescale depending on the cloud liquid water content and drop size distribution. Therefore, as $f_{(g)} \rightarrow 0$ and $\delta_{(g)} = \delta_{(g)o} - \varepsilon_{l/v}$ and $\delta_{(aq)} = \delta_{(g)o}$ (Fig. 3).

In an open Rayleigh distillation, an infinitesimal chemical and isotopic equilibrium is achieved between the products and reactants, or phases, but the new product (or phase) is removed from the system (Criss, 1999). Analogous to the above example, a rain droplet falling through an atmosphere containing gas HNO_3 and using the same notation as above, the $\delta_{(g)}$ and $\delta_{(l)}$ values are a function of the fraction of HNO_3 gas remaining:

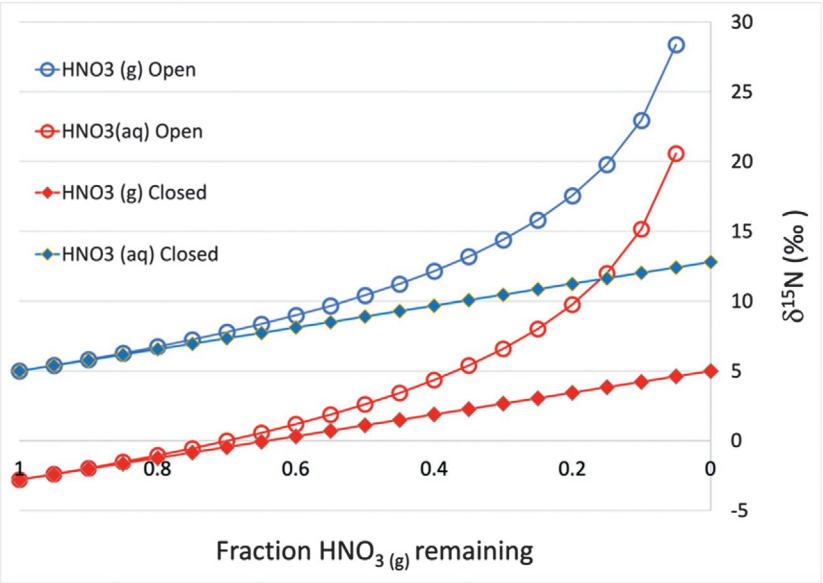

Fig. 3 The change in $\delta\ ^{15}N$ of gas phase HNO_3 (g) and aqueous phase HNO_3 (aq) as a function of the fraction of HNO_3 remaining in the gas phase for an open or closed system applying the Rayleigh distillation model and using a starting $\delta\ ^{15}HNO_3$ of +5‰. An $\varepsilon_{aq/g}$ of –6.7‰ was used assuming that diffusion across a stagnant layer at the droplet-atmosphere interface was the isotope fractionating process.

$$\delta_{(g)} = \delta_{(g)o} + \ln\left(f_{(g)}\right) \bullet \varepsilon_{v/l} \tag{16}$$

$$\delta_{(l)} = \delta_{(g)o} + \left(\ln\left(f_{(g)}\right) + 1\right) \bullet \varepsilon_{v/l} \tag{17}$$

Such a hypothetical case might be a series of small droplets falling through an atmosphere with high levels of $HNO_{3\ (g)}$, with the uptake limited by the volume of water. The residual $HNO_{3(g)}$ becomes progressively enriched in ^{15}N, as would each succeeding droplet (Fig. 3).

Tropospheric NO_y isotopologues

Measurements of N and O isotopes in NO_y compounds in the atmosphere must be interpreted in the context of all of these above-mentioned processes. For example, the $\delta^{15}N$ of tropospheric HNO_3 will be a function of the $\delta^{15}N$ values of the precursor NO_x sources, the KIE, EIE, VPIE, and PHIFE occurring during the reactions that convert NO_x into HNO_3, and what fraction of the NO_x is converted into HNO_3. In a simple case, such as a NO_x plume where >95% of the NO_x is converted into HNO_3 within the plume, then the plume $\delta^{15}HNO_3$ should be roughly equal to the $\delta^{15}NO_x$ (i.e., closed Rayleigh model). Conversely, after a major rainfall event, where the majority of N pollutants have been removed, new HNO_3 being formed from new NO_x emissions will have a significantly different $\delta^{15}N$ value compared to the NO_x source due to the KIE, EIE, VPIE, and PHIFE occurring during oxidation and because only a small fraction of total NO_y is HNO_3 at this point. The same holds for oxygen isotopes, but with significant differences. The oxygen isotope composition of NO_x emitted by a particular source during the day is quickly lost during photochemical recycling. The photolysis lifetime of NO_2 is a few minutes during peak sunlight, while the lifetime of HNO_3 production is on the order of hours to days depending on the oxidant load. Thus, $\delta^{18}O$ ($\Delta^{17}O$) values of daytime HNO_3 is controlled by the oxidation chemistry, with sources playing almost no role. This is not the case during the night when photolysis is no longer acting as the "isotopic scrambler," and NO_x sources can influence $\delta^{18}O$ and $\Delta^{17}O$ of HNO_3 produced at night. Therefore, it is important to understand the $\delta^{18}O$ and $\Delta^{17}O$ values of the main oxidants in the troposphere.

Isotopologues of tropospheric oxidants

Isotopologues of tropospheric O_2

As the most abundant oxidant in the atmosphere, molecular oxygen (O_2) is key to several reaction schemes that influence the $\delta^{18}O$ and $\Delta^{17}O$ of many reactive atmospheric isotopologues. It is widely accepted that tropospheric O_2 has an essentially constant $\delta^{18}O$ value of +23.4‰ (Dole et al., 1954; Kroopnick and Craig, 1972). This +23.4‰ value (Fig. 4) is the result of the "Dole effect" (Bender et al., 1994), the balance between the production of O_2 by photosynthesis, which roughly equals the $\delta^{18}O$ of water at the chlorophyll-air interface, and isotope enrichment of O_2 that occurs during respiration (ε ~+20‰). Deviations from the +23.4‰

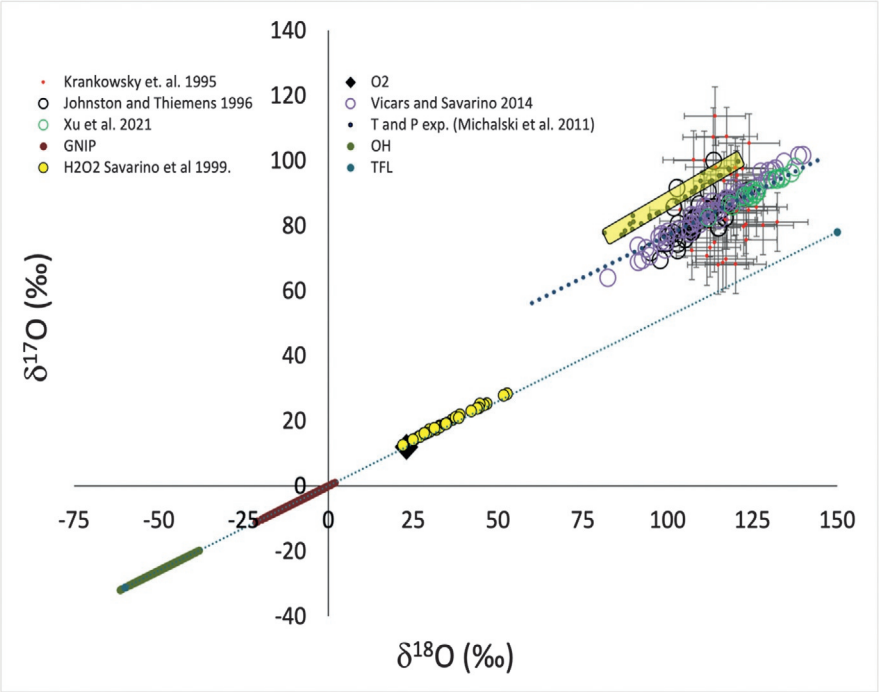

Fig. 4 Dual oxygen isotope ratio plot of the main tropospheric oxidants: O_2, H_2O, OH, O_3 and H_2O_2. Tropospheric O_2 (black triangle) has a nearly constant $\delta\,^{18}O$ value of 23.4‰ (Dole et al., 1954) and only per meg variation in $\Delta^{17}O$ (Luz and Barkan, 2005). The tropospheric water vapor range is based on 1300 measurements at GNIP sites between 43°S and 70° and assuming $\delta\,^{17}O = 0.52\delta\,^{18}O$ based on triple oxygen isotope analysis of meteoric waters by (Meijer and Li, 1998). The $\delta\,^{18}O$ and $\delta\,^{17}O$ of OH is based on the EIE between OH and tropospheric water vapor using e values based on a's calculated in Walters and Michalski (2016a,b). There is a $\Delta^{17}O$ of 1–2‰ in rainwater H_2O_2 (Savarino and Thiemens, 1999a,b) that is obscured by the graph scale. The measured $\delta\,^{18}O$ and $\delta\,^{17}O$ of tropospheric O_3 (open circles) are from authors shown in the chart legend. The measurement error bars are the size of the symbols except for Krankowsky et al., which are shown explicitly. The envelope of $\delta\,^{17}O$ and $\delta\,^{18}O$ predicted by the pressure and temperature dependence of the ozone isotope effect for typical tropospheric T and P is shown as the transparent yellow bar. Most tropospheric O_3 falls on a slope ~0.6 line offset by ~27‰ (purple dashed line) from the mass dependent terrestrial (isotope) fraction line (TFL) that passes through atmospheric O_2 (black diamond, line) and SMOW at the x-y intercept.

value arise when O_2 becomes isolated, either below the ocean mixed layer, inside leaves, or in soil pore space, where either photosynthesis or respiration is more rapid than mixing with the free atmosphere. Tropospheric O_2 does have "per-meg" ($1/10^6$ = parts per mega) size variations in $\Delta^{17}O$ values (Luz and Barkan, 2000; Luz et al., 1999) due to isotope exchange between CO_2 and $O^1(D)$ in the stratosphere. But from the perspective of understanding reactive tropospheric isotopologues of NO_y, assuming O_2 has an $\delta^{18}O = +23.4‰$ and $\Delta^{17}O = 0$ seems a valid approximation. In the gas phase the direct oxidation of NO_x and SO_x by O_2 is slow relative to oxidation by radicals and is therefore generally considered unimportant. This is not the case for some stack emissions where complete S and N oxidation by O_2 occurs during combustion, generating "primary" SO_4^{2-} and NO_3^- via O_2 or O_2 derived radicals (Holt et al., 1982; Proemse et al., 2012). Indeed, stack aerosol NO_3^- with $\Delta^{17}O$ values close to zero and SO_4^{2-} with elevated $\delta^{18}O$ are evidence of this in stack oxidation by O_2 (Holt et al., 1982; Proemse et al., 2012). More importantly, O_2 is utilized during tropospheric photochemistry as a functional group in radical propagation. For example, H radicals (from the CO + OH➔CO_2 + H reaction) immediately combine with O_2 to form a hydroperoxyl radical (HO_2) that can oxidize NO and SO_2 (Monks, 2005), transferring an oxygen atom and likely inducing some KIE. Thus, it has been hypothesized that oxygen atoms from radicalized O_2 get incorporated into NO_3^- and SO_4^{2-} during NO_x and SO_x oxidation and inherit a proportion of O_2's isotopic value (Lyons, 2001; Michalski et al., 2011). Likewise, OH oxidized organic compounds (●R) form organic radicals that rapidly combine with O_2 to form alkyl peroxy radicals (RO_2) that oxidize NO into NO_2 (Fig. 1, R16). Presumably, this transfers an O atom derived from O_2 to NO_2 with some KIE. O_2 also plays a role in the aqueous phase metal-catalyzed oxidation of S(IV) that has been recognized as a significant S oxidation pathway, particularly in highly polluted urban centers (Alexander et al., 2009b; Sofen et al., 2011). Thus, it is clear that the $\delta^{18}O$ (+23.4‰) and $\Delta^{17}O$ (0‰) of O_2 must impact the $\delta^{18}O$ and $\Delta^{17}O$ values of reactive tropospheric isotopologues.

Isotopologues of tropospheric H_2O

The $\delta^{18}O$ of tropospheric water varies widely across the planet, caused by competing isotope fractionations occurring during evaporation and condensation, and plays in important role in the $\delta^{18}O$ and $\Delta^{17}O$ compositions of reactive N isotopologues. The Global Network of Isotopes in Precipitation (GNIP) has shown that the $\delta^{18}O$ of tropospheric water is typically 0 to −30‰ with

respect to ocean water (Fig. 4) but can range from extremely negative values at the poles (~ −60‰) to slightly positive values (~+5‰) in arid environments (Meijer and Li, 1998). Water does have small, per-meg level variations in $\Delta^{17}O$ values that are caused by different mass-dependent slopes for the KIE and EIE occurring during evaporation (Barkan and Luz, 2007; Luz et al., 2009; Uemura et al., 2010). But permeg $\Delta^{17}O$ is far below current $\Delta^{17}O$ analytical techniques for reactive tropospheric isotopologues, therefore a $\Delta^{17}O$ ~0‰ assumption seems valid for the current discussion. Water absorbed to aerosol surfaces, sometimes called a quasi-liquid layer, likely plays a role in the $\delta^{18}O$ and $\Delta^{17}O$ of $NO_{3\bar{atm}}$ via (R9) the heterogeneous N_2O_5 + aerosol(aq) ➔ $2HNO_3$ reaction (Chang et al., 2011) when liquid water is incorporated into HNO_3. The $\delta^{18}O$ of the vapor H_2O is negative with respect to the liquid due to the EIE between the two phases (Griffis et al., 2016) and the size of EIE is a function of temperature and ranges from about −11.7‰ to −8‰ over temperature ranges typical of the troposphere (273-315 K). Water vapor can be incorporated into $NO_{3\bar{atm}}$ via the $N_2O_5 + H_2O$ ➔ $2HNO_3$ reaction but this reaction is slow with respect to the N_2O_5 heterogeneous reaction. More importantly H_2O vapor can undergo isotopic exchange with OH radicals (see below) and be incorporated in $NO_{3\bar{atm}}$ via R5. Thus, it is clear that water, both as a liquid and a gas, directly impacts reactive tropospheric isotopologues $\delta^{18}O$ and $\Delta^{17}O$ values.

Isotopologues of tropospheric O_3

There are only four studies that have measured the oxygen isotopic composition of tropospheric ozone (Fig. 4) utilizing two different analytical methods. Johnston and Thiemens (1997) and Krankowsky et al. (1995) used cryogenic trapping of whole air and separation to isolate O_3, then decomposed it into O_2 and measure that by dual inlet IRMS (Johnston and Thiemens, 1997; Krankowsky et al., 1995). Johnston and Thiemens (1997) observed tropospheric O_3 $\delta^{18}O$ values (from 3 different sites) ranging from 102 to 120‰ (relative to SMOW) with a mean of 107 ± 7‰ and $\Delta^{17}O$ values ranging from 20 to 35.8‰. Krankowsky et al. measured similar O_3 $\delta^{18}O$ values but with a higher mean (116 ± 6‰) and a wider range of 103‰ to 132‰. Krankowsky et al. did not report their $\Delta^{17}O$ values but based on data extracted from their Fig. 4, their $\Delta^{17}O$ had a much higher range relative to Johnston and Thiemens, from 6‰ to 54%. This may, in part, be due to their high analytical uncertainty in both $\delta^{18}O$ (±10‰) and $\delta^{17}O$ (±12‰). Neither of these studies reported the ambient temperature and pressure during the sampling period, therefore it is difficult to make a direct comparison between these reported values and those predicted by lab experiments. A more recent technique for measuring O_3 isotopes takes advantage of the reaction of O_3 on nitrite-coated filters to produce nitrate and subsequent NO_3^- isotope analysis (Vicars et al., 2012; Xu et al., 2021). Along a ship track that spanned from Patagonia to northern France, Vicars and Savarino (2014) measured a similar O_3 $\delta^{18}O$ range and mean (113 ± 13‰) as the cryogenic studies but a much narrower $\Delta^{17}O$ range (25.8 ± 3‰) (Vicars and Savarino, 2014). Xu et al. (2021) has recently reported a slightly higher $\delta^{18}O$ mean (127 ± 7‰) on a limited data set from Japan ($n = 19$) but like Vicars and Savarino, a relatively narrow $\Delta^{17}O$ range (25.1 ± 0.8‰).

The observed tropospheric O_3 $\delta^{18}O$ and $\Delta^{17}O$ values are at slight odds with the values expected based on tropospheric temperatures and pressures (Fig. 4). Numerous laboratory experiments have shown that the magnitude of both the mass-dependent and mass-independent isotope fractionation during O_3 formation is a function of both the ambient temperature and pressure (see reviews by Thiemens, 2005; Mauersberger et al., 2003). Michalski et al. used the experimental data to derive simple temperature (in K) and pressure (in torr) equations that predict $\delta^{18}O$ and $\Delta^{17}O$ for ozone produced in the troposphere (Michalski et al., 2011).

$$\delta^{18}O = (-0.028 \bullet P + 134.8) + 0.52 \bullet (T - 321) \quad (18)$$

$$\Delta^{17}O = \left(78.8 \bullet P^{-0.122}\right) + 0.06 \bullet (T - 321) \quad (19)$$

Assuming a planetary boundary layer extending from the surface to 4 km (760 to 220 Torr) and a temperature range between 330 K and 260 K, then tropospheric O_3 $\delta^{18}O$ values should range between ~80‰ to 120‰. This is in good agreement with most of the tropospheric O_3 $\delta^{18}O$ observations, although some of the nitrite technique data appears biased to higher values. This bias could be a consequence of two factors. First, ozone in the troposphere is highly reactive towards NO_x, VOCs, and surfaces, and assuming isotopically light O_3 reacts faster than heavy, typical for KIEs, then residual O_3 $\delta^{18}O$ would become elevated relative to the initial (formation) value. Second, it is possible there may be some mass-dependent isotope effects occurring in the nitrite + O_3 reaction during collection, which would explain the lower $\delta^{18}O$ values in the cryogenic collection data. The O_3 $\Delta^{17}O$ predicted for tropospheric P and T is between 32‰ and 36‰ (Fig. 4), significantly higher than those observed using the filter technique and in most of the cryogenic data. The narrow $\Delta^{17}O$ minimum and maximum spread for the P and T experiments (4‰) agrees well with the spread observed by Vicars and Savarino (3‰), but their absolute $\Delta^{17}O$ values are roughly 10‰ lower than those predicted by the experiments. Likewise, only 4 data points in the.

Johnston and Thiemens study are near the experimental values, which when excluded, brings the study into an agreement with Vicars and Savarino and Xu et al. The Krankowsky et al. $\Delta^{17}O$ also averages 25‰ but this is a fortuitous consequence of poor precision rather than accurate $\Delta^{17}O$ measurements.

The cause of the discrepancy between observed tropospheric O_3 $\Delta^{17}O$ values and those predicted by laboratory experiments is unclear. The obvious possible cause is the difference in environmental conditions in the experiments compared to the troposphere. The experiments were carried out in either pure O_2 or O_2 in an inert bath gas using high-energy UV or electrical discharge to disassociate O_2. In contrast, ozone in the troposphere is produced by NO_2 photodissociation at visible and low-energy UV wavelengths. This particular potential bias seems unlikely because experiments examining NO_x-O_3 isotopic photo-equilibrium

showed that the O_3 isotope composition was the same as those in the pure O_2 experiments (Michalski et al., 2014). The troposphere, however, also has a number of trace gases that are highly reactive with ozone, and there is potential for some unknown oxygen isotope exchange reactions to occur during photochemical cycling in the troposphere.

Another important consideration concerning the $\Delta^{17}O$ of tropospheric O_3, and its ability to transfer oxygen atoms to other compounds during oxidation reactions, is the isotopic difference between the central and terminal atoms within the O_3 molecule. Like water, ozone is a bent, 3-atom molecule with C_{2V} symmetry and both experiments and theory suggest that the isotopic composition of the oxygen atoms within O_3 are not equal. When the minor isotope, either ^{17}O or ^{18}O, is substituted at the terminal end of an ozone molecule it reduces ozone's symmetry from C_{2V} to C_S. It is in this symmetry breaking that the mass-independent isotope effect is believed to be derived (Gao and Marcus, 2001), suggesting the terminal atom will contain all the $\Delta^{17}O$ anomaly. Experiments have shown this to be the case (Bhattacharya et al., 2008; Michalski and Bhattacharya, 2009) and that the $\Delta^{17}O$ value of the terminal oxygen atom is 1.5 times that of the bulk O_3. This is important because it is the terminal atom that is transferred to NO_2 during NO ozone oxidation (R1) and controls the $\Delta^{17}O$ of higher NO_y oxides (see Section "Oxygen isotopes fractionations during the production of NO_y and tropospheric observations"). Based on the observed tropospheric O_3 $\Delta^{17}O$, the value of the terminal oxygen atom is currently assumed to be $39 \pm 2‰$ (Albertin et al., 2021). This is in good agreement with NO_x-O_3 photochemical equilibrium experiments that previously showed NO_2 reached a steady state $\Delta^{17}O$ value of $39.3 \pm 1.9‰$ and $\delta^{18}O$ values of $84.2 \pm 4‰$ (Michalski et al., 2014).

Isotopologues in the tropospheric HO_x cycle

The tropospheric water vapor also plays an important role in the $\delta^{18}O$ and $\Delta^{17}O$ values of reactive isotopologues indirectly through the HO_x cycle (R15a, R15b and R20). Water vapor is the reactant used to produce the OH radical (R15a, R15b) a vital oxidant in atmospheric chemistry. It oxidizes all important trace gases including CO, NO_2, and SO_2 thus influencing the isotope composition of photochemically produced CO_2, NO_3^- and SO_4^{2-}. OH is produced when ozone photolysis by UV radiation produces $O^1(D)$ that reacts with H_2O (R15a, R15b).

$$O_3 + h\nu \rightarrow O_2 + O^1(D) \quad \text{(R15a)}$$

$$O^1(D) + H_2O \rightarrow 2\,OH \quad \text{(R15b)}$$

$$H^{18}OH + OH \leftrightarrow H_2O + {}^{18}OH \quad \text{(R20)}$$

Since the $O^1(D)$ is derived from O_3 dissociation, theoretically OH should initially have high $\Delta^{17}O$ and $\delta^{18}O$ values, roughly half of those found in O_3 since H_2O $\delta^{18}O$ and $\Delta^{17}O$ values are roughly zero. However, experiments have shown that there is an isotope exchange between OH and gaseous H_2O (Greenblatt and Howard, 1989) and that due to H_2O's large mixing ratio (~ 0.01) OH's initial isotope composition can potentially be erased through this EIE (Michalski et al., 2011). This suggests that little of O_3 $\Delta^{17}O$ is transferred from OH to compounds during OH addition reactions.

Hydrogen peroxide (H_2O_2) is an important oxidant in the aqueous phase and its isotopic composition has relevance for oxygen isotopes during SO_4^{2-} production by SO_2 oxidation in clouds, fog and rain. To date there has only been one study on the $\delta^{18}O$ and $\Delta^{17}O$ of atmospheric H_2O_2. Savarino and Thiemens measured H_2O_2 in coastal rain collected in San Diego, USA over a 4-month period (Savarino and Thiemens, 1999a). They found $\delta^{18}O$ values ranging between 22 and 53‰ versus SMOW and $\Delta^{17}O$ values that ranged from 1.2 to 2.4‰. The origin of the elevated $\delta^{18}O$ and $\Delta^{17}O$ values in H_2O_2 is unresolved but similar effects have been generated in water vapor discharge experiments (Savarino and Thiemens, 1999b) and may be related to HO_x chemistry. The recent detection of significant HO_x production during lightning discharges in convective storms (Brune et al., 2021) is a possible connection to observed $\Delta^{17}O$ in rainwater H_2O_2 and the discharge experiments (Savarino and Thiemens, 1999b). Since H_2O_2 is produced via OH chemistry, the observed positive $\Delta^{17}O$ and high $\delta^{18}O$ values in H_2O_2 possibly suggests that the OH + H_2O isotope exchange may not reach full equilibrium. Under high NOx (10 ppbv) and/or low water mixing ratios (5E-3) the OH reactivity rates can become comparable to the isotope exchange rate, but these cases are rare (Morin et al., 2008). What has been demonstrated is that some fraction of the $\Delta^{17}O$ observed in rain and aerosol SO_4^{2-} is due to the transfer of an O atom from H_2O_2 to SO_4^{2-} during aqueous phase SO_2 oxidation (Savarino et al., 2000), thus $\Delta^{17}O$ can be used to trace SO_2 oxidation by H_2O_2 and O_3.

Isotopes of N in precursor gases NO_x and NH_3

NO_x, primarily as NO, is emitted by a number of natural and anthropogenic processes that have a range of isotope compositions. Likewise, there are a number of natural and anthropogenic processes that emit NH_3 with a significant range of $^{15}N/^{14}N$ isotope compositions. Here only measurements of $\delta^{15}NO_x$ (Fig. 5) collected directly (or as close to directly as possible) from the source are discussed to the exclusion of ambient sampling near sources or using proxies (tree rings, lichen) because there is potential for chemical and isotopic alteration of NO_x over timescales shorter than, or comparable to, atmospheric transport from the source to the sampling/proxy location.

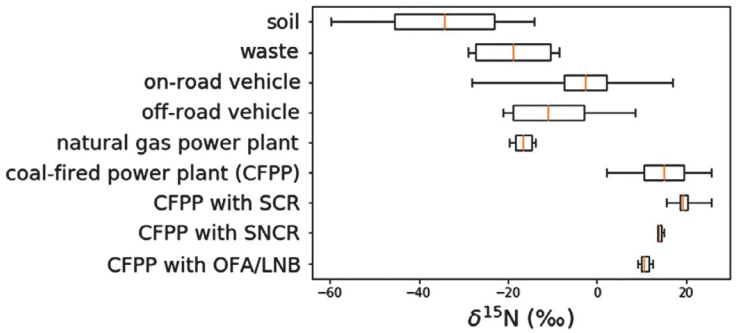

Fig. 5 The $\delta^{15}N$ distributions of NO_x collected directly from various sources as discussed in the text. There is clear $\delta^{15}N$ differences between three of the main NO_x sources: Soils, vehicles, and coal fired power plants with different NO_x reduction technologies. From Fang H and Michalski G (2022) Assessing the roles emission sources and atmospheric processes play in simulating $\delta^{15}N$ of atmospheric NO_x and NO_3^- using CMAQ (version 5.2.1) and SMOKE (version 4.6). *Geoscientific Model Development* 15(10): 4239–4258, https://doi.org/10.5194/gmd-15-4239-2022.

The $\delta^{15}N$ of soil NO_x

NO emitted by soils as a by-product of nitrification and denitrifications has very negative $\delta^{15}N$ values. Nitrification is the stepwise microbial oxidation of NH_4^+ to NO_3^- and denitrification is the stepwise microbial reduction of NO_3^- to N_2, and in both processes ^{14}N reacts preferentially (Hogberg, 1997). During both processes NO (and N_2O) are reaction intermediates and as gases can diffuse across cellular membranes and diffuse out of soil and collecting known a "soil NOx". Li and Wang first reported $\delta^{15}NO$ ranging from −49 to −28‰ in lab incubation fertilization experiments using cropland soils, with more negative values emitted immediately after fertilization and the less negative values occurring several weeks later (Li and Wang, 2008). They suggested this was a shift of NO produced as a by-product of nitrification to that derived from denitrification. Felix and Elliott only studied livestock waste emissions (cows and turkeys) using passive samplers and found $\delta^{15}N$ from −29‰ to −8.5‰ (Felix and Elliott, 2014). Observations of seasonally dry grasslands that produced $\delta^{15}NO$ ~−43‰ 24 h after wetting were linked to nitrification (Homyak et al., 2016). NO emissions after fertilizer application (injected anhydrous and broadcast) in till and no-till fields had a range of $\delta^{15}N$ values from −20 to −45‰ with injected systems showing a less negative $\delta^{15}N$ values as a function of time since application (Miller et al., 2018). Field and lab fertilizer experiments generated $\delta^{15}NO$ ranging from −59.8 to −23.4‰, depending on the N substrates applied that induced either nitrification or denitrification (Yu and Elliott, 2017). Likewise, Su et al. found aerobic soil $\delta^{15}NO_x$ ranged from −62‰ to −50% while anaerobic soils ranged from −45‰ to −23‰ (mean −33 ± 7‰) with a small variability among ecosystem types (forest, grassland or agriculture) (Su et al., 2020). This significant $\delta^{15}N$ difference was attributed to NO_x being produced by nitrification in the aerobic soils and by denitrification in the anaerobic soil, which was supported by simultaneous $\delta^{15}N$ changes in soil NO_3^- and NH_4, similar to the results of Li and Wang. The emerging consensus is that the ^{15}N enrichment factor is more negative for nitrification (~ −60‰) than for denitrification (~30‰) but in either case, the extremely negative soil $\delta^{15}NO$ values may be useful as a tracer of the relative importance of nitrification/denitrification in regional NO_x budgets.

The $\delta^{15}N$ of biomass burning NO_x

The $\delta^{15}NO_x$ produced during biomass burning is a function of the $\delta^{15}N$ of the biomass N. Laboratory experiments by Fibiger and Hastings (2016) showed $\delta^{15}NO_x$ generated by biomass burning was mainly a function of the biomass $\delta^{15}N$ value, but also of how the burn emission were sampled. When emissions were collected as part of a rising plume, the $\delta^{15}NO_x$ was about +2‰ relative the $\delta^{15}N$ of the biomass burned. When emissions were allowed to sit for 1–2 h inside the chamber, the $\delta^{15}NO_x$ was about 1/2 the $\delta^{15}N$ value of the biomass burned, possible due to secondary chemistry occurring while NO_x resided in the chamber. This is a good example of how quickly chemistry can alter the initial $\delta^{15}NO_x$ value of an emission source. In a similar study, direct NO_x emitted by laboratory fires that burned various biomass materials from the western US had $\delta^{15}NO_x$ ranges from −4.3‰ to +7.0‰ and correlated with the $\delta^{15}N$ of the fuel (Chai et al., 2019) and similar results have been found in NO_x generated in biomass-burning cookstoves (Shi et al., 2022; Zong et al., 2022). The $\delta^{15}N$ of above-ground biomass averages 0.9‰ with 95% of the samples falling within a range of −7.8‰ to 8.7‰ (Amundson et al., 2003; Craine et al., 2015). Thus, the $\delta^{15}NO_x$ generated by wildfires will therefore be a function of the $\delta^{15}N$ of the particular biome being burned but globally should center around 0 ± 8‰.

The $\delta^{15}N$ of lightning NO_x

The $\delta^{15}NO_x$ produced from lightning is poorly constrained. Lightning produces peak temperatures in excess of 30,000 K for a few microseconds mostly by ohmic heating (Orville, 1968). Subsequent expansion, radiation, and conduction, cools the discharge channel to 3000–4000 K plasma with high concentrations (order of 1–20%) of O, NO, OH, NO and N radicals produced by the Zel'dovich mechanism (Bhetanabhotla et al., 1985; Goldenbaum and Dickerson, 1993; Hill, 1979). Rapid cooling of this hot channel occurs over next milliseconds and "freezes out" the NO, prohibiting attaining thermal equilibrium with N_2 and O_2 and

producing ppb_v level of NO_x along the flash path (Chameides et al., 1977; Pollack et al., 2016). Using EIE from Urey and Greiff (1935), Ingerson postulated that lightening NO_x might be −15‰ (at 375C) depending on when $^{15}NO + N_2 \leftrightarrow {}^{15}N_2 + NO$ equilibrium ceased but at higher temperatures (∼ 1200 K) the EIE should become negligible with $\delta^{15}N < 1.7‰$ (Ingerson, 1953; Urey and Greiff, 1935). This assumption is questionable because combustion NO_x, also occurring at high temperatures shows a significant KIE rather than an EIE. A single set of experiments designed to simulate lightning, but with few experimental details, showed air flowing through a spark discharge produced a $\delta^{15}N$ of nitrate (NO_x) at −0.5 to +1.4‰ (Hoering, 1957).

The $\delta^{15}N$ of NO_x from internal combustion engines (ICE) and ship emission

The $\delta^{15}NO_x$ emitted by vehicles varies depending on the vehicle type, particularly whether it is equipped with a NO_x reduction catalytic converter (CC) and the driving conditions. Similar to lightning, NO_x is produced in ICEs via the Zel'dovich mechanism. ICE's that lack CCs, such as lawn care equipment and older vehicles tend to produce negative $\delta^{15}NO_x$ values (Walters et al., 2015b, c). This has been interpreted as a KIE occurring during the Zel'dovich mechanism with the ^{14}N reacting preferentially due to its higher zero-point energy. Similar to older vehicles without CCs, new vehicles emitted negative $\delta^{15}NO_x$ during initial startup but the $\delta^{15}NO_x$ became less negative and even positive as the engine operation time increased (idling or driving). This phenomenon was explained by a KIE or EIE occurring during NO_x reduction on the CC surface where $^{14}NO_x$ was preferentially reduced to N_2 leaving $^{15}NO_x$ in the NO_x exhaust stream (Walters et al., 2015b). These results have been replicated by a number of studies in several countries. Similar isotope effects have been observed in diesel engines that utilize ammonia-based selective catalytic reduction (SCR) technology (Walters et al., 2015c). Recently, the $\delta^{15}N$ emission values of the main and auxiliary engines from 9 vessels were − 18.5 ± 10.9 ‰ with a negative logarithmic relationship with NOx concentrations that again showed the isotope effect of emission control technology (Sun et al., 2023).

The $\delta^{15}N$ of NO_x from electrical generating units and industry

Electrical generating units (EGUs) and industrial/residential boilers produce $\delta^{15}NO_x$ values that depend on the combustion type (temperature), fuel source, and whether any NOx reduction technologies are utilized on a particular emission stack. Felix et al. (2012) collected NO_x from EGU stacks and found the $\delta^{15}NO_x$ ranged from 9‰ to 26‰, significantly higher than that of other measured NO_x emission sources (Felix et al., 2012). The $\delta^{15}NO_x$ emitted by coal burning in EGUs or during home heating is, like biomass burning, partially a function of the $\delta^{15}N$ content of the coal. The $\delta^{15}N$ of nitrogen in coal are unique depending on its place of origin but typically ranges between +4‰ and − 4‰ (Xiao and Liu, 2011). Coal combustion can also produce thermal NO_x from reactions between nitrogen and oxygen radicals produced at high temperatures. Depending on the country or age of a power plant it may or may not be equipped with NO_x selective reduction technology. EGU stacks burning coal with a $\delta^{15}N = +2‰$ produced $\delta^{15}NO_x$ of ∼ +10.5‰ when the SCR was turned off but +20‰ when the SCR was active (Felix et al., 2012), indicating a KIE or EIE during SCR was enriching NO_x isotopes, similar to vehicle CC. In the US and Europe, natural gas has been replacing coal as a fuel source in coal burning EGUs and natural gas turbines have become an important source of electricity during peak demand because they can be fired and stopped on much shorter timescales compared to traditional boilers. Since there is no nitrogen in natural gas, NO_x is likely produced exclusively by the Zel'dovich mechanism during gas combustion. The $\delta^{15}NO_x$ values measured in gas fired EGUs (−17.9‰) and gas home heaters (−15.5‰) is consistent with this hypothesis (Walters et al., 2015c). Sampling from a nitric acid production plant had NO_3^- (and likely NO_2) $\delta^{15}N$ of −150‰ that was attributed to a Rayleigh distillation during NO_2 hydrolysis (Heaton, 1987) which is the synthesis method for producing commercial HNO_3 (Michalski et al., 2015).

Less is known about the $\delta^{15}NO_x$ values in other important combustion NO_x sources. Locomotives, fracking pumps, and various in-flight aircraft can be significant NO_x sources regionally and none of these sources typically have any NO_x reduction technology. Given that they are producing thermal NO_x similar to ICE and natural gas boilers, it is probable that ships, locomotives, and aircraft produce NO_x in the −10 to −15‰ but this should be confirmed by direct collection of NO_x emitted by these sources. Less is known about other NO_x sources such as other industrial/manufacturing processes, home oil heating, or waste management, and miscellaneous sources that account 25% of NO_x emissions in the USA.

The $\delta^{15}N$ of tropospheric NO_y

The isotopic composition of the final products formed by the photochemical transformation of NO_x and NH_3 will usually be different from the composition of the emitted reactants discussed in the previous section. This is a consequence of three effects: First, the mixing of the isotopic composition of the various reactant sources, second the isotope fractionation associated with the EIE, KIE, VPIE, and PHIFE as the compounds are oxidized, and third the fraction of the reactants converted into products (see Section "Stable isotope abundance nomenclature, fractionations, and mass balance"). For $NO_x \rightarrow NO_y$ in an airmass, Eqs. (19) and (20) can be derived from the Rayleigh distillation equations for closed and open systems:

$$\delta^{15}N_{prod} = \Sigma f_i \bullet \delta^{15}NO_x + f_{NOx} \bullet \Sigma\, \varepsilon_{rxn\ i} \quad \text{(Closed; 20)}$$

$$\delta^{15}N_{prod} = \Sigma f_i \bullet \delta^{15}N_{react\ i} + (\ln f_{NOx} + 1) \bullet \Sigma\, \varepsilon_{rxn\ i} \quad \text{(Open; 21)}$$

Here, $\delta^{15}N_{prod}$ is the value of the product (e.g., NO_3^-, HNO_3, HONO), f_i is the mole fraction of each NO_x source (i) relative to the airmass total NO_x, $\delta^{15}NO_x$ is $\delta^{15}N$ value of each source (i) in the mixture, $f_{NOx.}$ is the fraction of the reactant NO_x remaining in the

airmass, and $\Sigma\varepsilon_{rxn\ i}$ is the total isotopic enrichment associated with the relevant chemical reactions (i) diagramed in Fig. 1. The $\Sigma\varepsilon_{rxn\ i}$ has been termed simply ε_{oxid}, the total isotope enrichment associated with NO_x oxidation (Song et al., 2021), but it should be noted that ε_{oxid} will be different for different products (e.g., HONO compared to HNO_3) and will likely change for any single product for different environmental conditions, such as differences in sunlight hours and VOC emission rates.

Some limiting cases in this reactive Rayleigh model are worth noting. In the case of a closed system when nearly all NO_x is fully oxidized (as f_{NOx} approaches zero) and the $f_{NOx}\bullet\Sigma\varepsilon$ term goes to zero and the product $\delta^{15}N$ will equal the $\delta^{15}N$ mass balance of the NO_x sources. A hypothetical example of such a condition might be a meteorologically stagnant, highly polluted urban environment with high O_3 levels or a concentrated NO_x plume. In such cases, the product $\delta^{15}N$ value (mainly NO_3^-) could be used to constrain the local NO_x source budget. In a high f_{NOx} case ($f_{NOx} \sim 1$), in both open and closed systems, the NO_3^- the product will be enriched by $\Sigma\varepsilon_{rxn\ i}$. An example of a high f_{NOx} condition might be an air mass immediately after a major rainfall event where all $NO_{3\bar{a}tm}$ is removed by wet deposition and freshly emitted NO_x is just beginning to be oxidized into new $NO_{3\bar{a}tm}$. If mechanistic isotope models (Section "Explicit mechanistic models for simulating $\delta^{15}N$, $\delta^{18}O$, and $\Delta^{17}O$") can accurately predict $\Sigma\varepsilon_{rxni}$ then the NO_y product $\delta^{15}N$ minus this photochemical isotope enrichment ($\Sigma\varepsilon_{rxn\ i}$) could be used to constrain the local NO_x source budget. For example, in their meta-analysis of $NO_{3\bar{a}tm}$ data, Song et al. used an empirical $\varepsilon_{oxid.} = 3.9 \pm 1.8‰$ to back out the $\delta^{15}NO_x$ sources and proposed that NO_x from soils emissions is underestimated in current NO_x budgets (Song et al., 2021). The intermediate cases are more complicated but measurements of NO_y concentrations can help constrain f_{NOx} and potentially be used to constrain NO_x sources. This complex, dynamic evolution of $\delta^{15}NO_3^-$ over time due the isotope effects occurring during conversion has recently been modeled using a simple photochemical box model (Fig. 6) (Fang et al., 2021). This isotope enabled photochemical model is discussed in Section "Modeling isotopologues of $NO_{3\bar{a}tm}$."

The $\delta^{15}N$ of tropospheric NO_y

There is mounting evidence that much of the $\delta^{15}N$ variations observed in NO_y are linked to isotope effects occurring during the photochemical oxidation of NO_x The photochemical effects influencing the $\delta^{15}N$ of NO_y compounds are observed in the direct measurements of $\delta^{15}NO_2$. Of the few studies that have measured $\delta^{15}NO_2$ most have found it to be depleted with respect to $NO_{3\bar{a}tm}$. Freyer et al. first measured the $\delta^{15}N$ of NO_2 sampled in Julich Germany between 1988 and 1991(Freyer et al., 1993) and showed a seasonal trend with high values in winter (+6.1‰ maximum) and a low values in summer (−8‰ minimum) and they were about 8‰ lower than co-collected pNO_3^-. They attributed this to NO_x photochemical recycling during the day (R1–R3) and NO-NO_2 EIE occurring at night. Passive sampling of NO_2 along a road-field gradient (6 sites) showed the summertime $\delta^{15}NO_2$ to be between −5 and −25‰ and between −10 and + 10 during the winter (November), with each site showing a ~15‰ increase from summer to winter (Redling et al., 2013). Dahal and Hastings (2016) reported a mean $\delta^{15}NO_2$ value of $-8.3 \pm 0.9‰$ in passively collected urban NO_2 during the summer and $-6.4 \pm 2‰$ in the winter (Dahal and Hastings, 2016). Passive NO_x collectors at 3 sites in in Canada showed $\delta^{15}NO_x$ varying from −5 to −30‰. On road and roadside NO_x in the New England region of the US, which represents a mixture of vehicle types and NO_x reduction technologies, had a fairly narrow range in $\delta^{15}N$ values of $-5 \pm 4‰$ (Miller et al., 2017), similar to the average values measured directly form vehicle tailpipes (Walters et al., 2015a). Walters et al. (2018) actively collected atmospheric NO_2 using denuder tubes in urban/suburban location (summer) and found a wider range, from

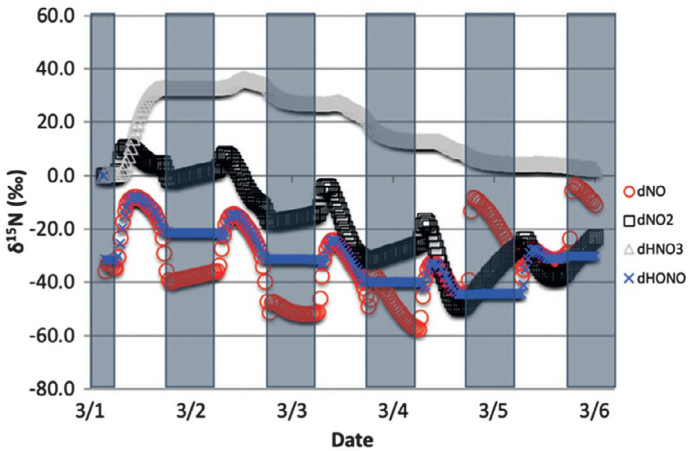

Fig. 6 The partitioning of ^{15}N between reactants (NO and NO_2) and products (HNO_3, HONO) over the course of a week predicted by the isotope-enabled photochemical box model $_{iN}$RACM (Fang et al., 2021). When the initial $\delta\ ^{15}N$ of NO_x was set to 0‰ and the $f_{NOx} \sim 1$,the initial HNO_3 produced during day 1 of the simulation, has $\delta\ ^{15}NO_3^- \sim \varepsilon_{oxid.}$ (About +30‰). After roughly a week, when $f_{NOx} \sim 0$ and $f_{HNO3} \sim 1$, the $\delta\ ^{15}NO_3^-$ approaches the initial $\delta\ ^{15}NO_x$ value. Simulations using $_{iN}$RACM have shown that $\varepsilon_{oxid.}$ Varies significantly for different environmental conditions.

+0.4‰ to −31.4‰ with a mean of −11.4 ± 6.9‰, similar to the mean of −10.2 ± 2.2‰ in Grenoble, France (Albertin et al., 2021). While all these $\delta^{15}NO_2$ are within the range of NO emission sources, they seem to be biased low for typical urban settings where vehicles (−3‰) and EGUs (+10 to +15‰) make up the majority of NO_x emissions. In particular, the data points around −30‰ would require NO being derived solely from soil emissions, which seems unlikely. These low $\delta^{15}NO_2$ are consistent, however, with an LCIE effect of −10‰ and a total NO_x isotope mass balance of sources of ~0‰.

Further evidence of photochemical isotope effects occurring during NOx oxidation is the seasonal trends in $\delta^{15}N$ of $NO_{3\bar{atm}}$. Freyer first noted the seasonal oscillation in the $\delta^{15}N$ of rainwater NO_3^- as well as in co-collected NO_2 and pNO_3^- (Freyer, 1978; Freyer, 1991). Most subsequent studies on $NO_{3\bar{atm}}$ collected longer than 1 year (Fig. 7) have noted the same trend, with elevated $\delta^{15}N$ in the winter and minimums in early summer (Hastings et al., 2003; Huang et al., 2021; Nelson et al., 2018; Wang et al., 2019; Bekker et al., 2023; Freyer, 1991; Riha, 2014; Kawashima, 2019) The trend follows seasonal trends in temperature and sunlight hours suggesting either, or both, of these factors could be playing a role in the observed $\delta^{15}NO_{3atm}$ seasonal trend. Temperature could be acting on the NO-NO_2 isotope exchange equilibrium (EX1) enrichment factor. Between 260 and 320 K $\varepsilon_{NO2/NO} = 0.20‰/K$ with an increasing $\delta^{15}NO_2$ with decreasing temperature (Begun and Fletcher, 1960; Walters and Michalski, 2015; Walters et al., 2016). Thus, the observed ~5‰ higher $\delta^{15}NO_{3\bar{atm}}$ values in winter could be explained by a 20 K seasonal change in temperature, which is not unreasonable, and has been observed in $\delta^{15}N$ of pNO_3^- as daily average temperature changed (Kawashima, 2019). Alternatively, sunlight that drives NO_y cycling also changes seasonally. Li et al. experimentally assessed the $\delta^{15}NO_x$ as a function of the Leighton cycle isotopic effect (LCIE), the combined isotope effects occurring during of R1, R2, and EX. 1 (Li et al., 2020). They found the $\Delta^{15}N_{NO2\text{-}NO}$ is controlled by LCIE in low NO_x environments and both LCIE and that the EX1 effect were important in high NO_x environments. The results suggested that more hours of darkness would lead to positive $\delta^{15}NO_2$ (with respect to source NO_x) while depleted $\delta^{15}NO_2$ (~ −10‰) is expected to occur when there are more daylight hours due to LCIE. This would be consistent with the observed seasonal $\delta^{15}N$ trend observed in $NO_{3\bar{atm}}$ since it is ultimately produced from NO_2.

Additional evidence of the photochemical effects influencing the $\delta^{15}N$ of NO_y compounds is the $\delta^{15}N$ difference between compounds when they are co-collected. Liu, Yin, and Song compiled a large dataset and showed that different NO_y compounds co-sampled in the same study have different $\delta^{15}N$ values (Fig. 8) indicating the EIE, KIE, VPIE, and PHIFE are partitioning ^{15}N during NO_x oxidation (Liu et al., 2020). Studies have shown that $\delta^{15}N$ values in $pNO_3^- > HNO_3 > NO_3^-(aq) > NO_2$, such as Bekker et al. who showed that pNO_3^- and HNO_3 had the same 10‰ seasonal change in $\delta^{15}N$ (peaking in winter; Fig. 7) but that HNO_3 was −3.8‰ relative to pNO_3 (Bekker et al., 2023). These differences are in general agreement with recent results from an ^{15}N enabled photochemical box model that showed EIE, KIE and PHIFE leads to $NO_{3\bar{atm}}$ being enriched relative to the precursor NO_x (up to 40‰) but also that this enrichment decreases as more NO_2 gets oxidized into $NO_{3\bar{atm}}$ (Fang et al., 2021). They were also in general agreement with chamber experiment examining the LCIE (Li et al., 2020). Kawashima et al. is the one study where NO_2 and HNO_3 $\delta^{15}N$ values were nearly the same (Fig. 8). But according to the methodology described therein, the NaOH-triethanolamine filter used to collect NO_2 was in front of the potassium carbonate impregnated filter to collect HNO_3 and it is likely a substantial fraction of HNO_3 would have reacted on the NaOH coating resulting in a $\delta^{15}N$ bias.

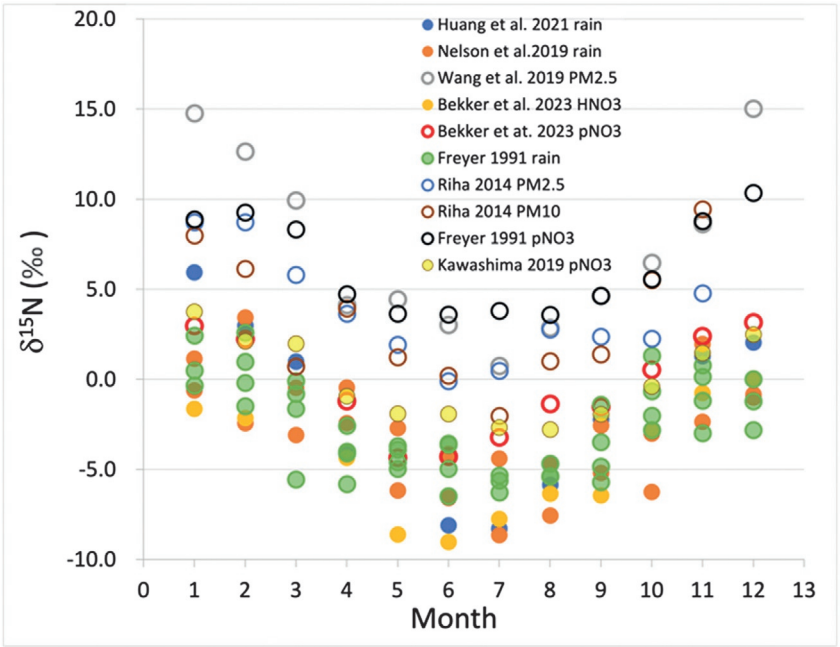

Fig. 7 The seasonal change of in the $\delta^{15}N$ of $NO_{3\bar{atm}}$ observed in northern hemisphere studies. Winter months have higher $\delta^{15}N$ values than the minimums observed in summer. Rain NO_3^- and gas HNO_3 (solid circles) tend to have lower $\delta^{15}N$ than pNO_3^-($PM_{2.5}$ and PM_{10}; open circles) but exhibit the same seasonal trend. Studies with more than 2 years of data are monthly averages for all years and Freyer's multiple icons are for 4 different sites in Germany.

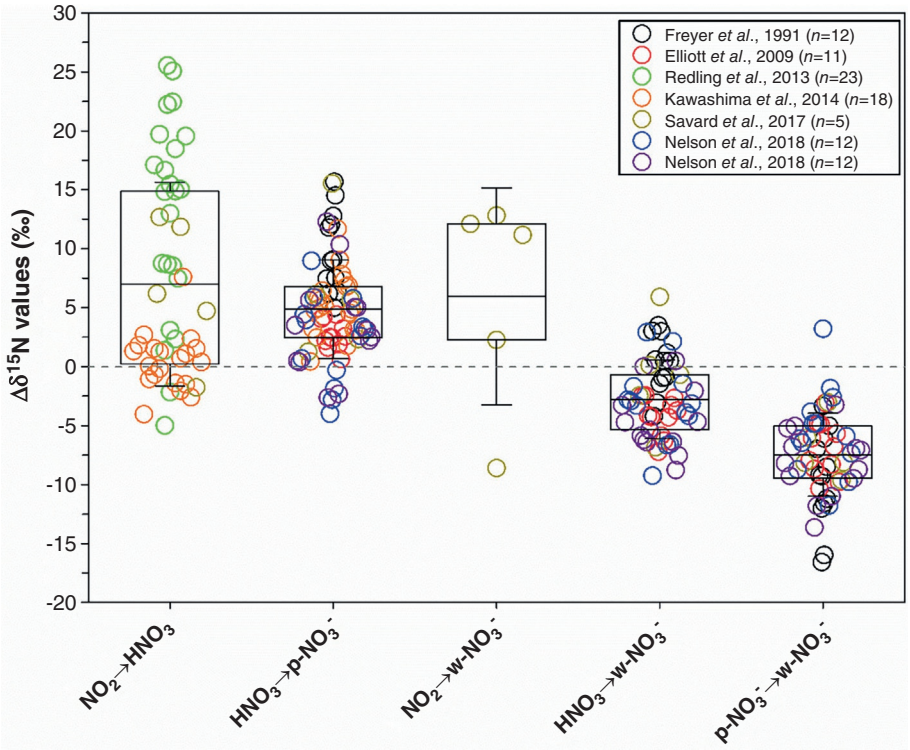

Fig. 8 Box and whisker plots of the $\Delta^{15}N = \delta\ ^{15}N_{prod} - \delta\ ^{15}N_{react}$ compiled by Liu et al. from various studies (inset) where two or more NO_y compounds were co-collected in the same study. For example, the $\delta\ ^{15}N$ value of HNO_3 is about 7‰ enriched relative to NO_2 and rain NO_3^- is about –8‰ relative to pNO_3^- in the same air mass. Permission from Liu XY, Yin YM, and Song W (2020) Nitrogen isotope differences between major atmospheric NOy species: Implications for transformation and deposition processes. *Environmental Science & Technology Letters* 7(4): 227–233. https://doi.org/10.1021/acs.estlett.0c00105.

The cause of the $\delta^{15}N$ differences between the different phases of NO_{3atm}^- is still an open question. One possible explanation is isotope effects occurring during phase changes, such as a HNO_3 diffusion effect. However, this seems unlikely because the isotope effect would be small and the high Henry's law constant for HNO_3 indicates it will effectively partition all HNO_3 into the liquid phase during washout. An alternative explanation is that cloud NO_3^- is formed from residual NO_x in an "aged" airmass. This could be due to different NO_x sources being transported from a distance, cloud aqueous NO_x chemistry, or "aged" HNO_3 incorporated into the cloud. Another possibility is that aqueous phase oxidation of NO_2 is more important than previously thought and produces low $\delta^{15}NO_3^-$ during rainfall (Liu et al., 2020). Regardless of the mechanism, it is hard to reconcile seasonal or hourly $\delta^{15}N$ differences in co-sampled NO_y to a change in NO_x sources and thus is more likely a result of photochemical isotope effects.

Oxygen isotopes fractionations during the production of NO_y and tropospheric observations

The same Rayleigh model use to describe $\delta^{15}N$ variations in tropospheric NO_y can be applied to the oxygen isotopic composition of NO_y products.

$$\delta^{18}O_{prod} = \Sigma f_i \bullet \delta^{18}O_{react\ i} + f_{NOx} \bullet \Sigma^{18}\varepsilon_{rxn\ i} \quad \text{(Closed; 22)}$$

$$\delta^{18}O_{prod} = \Sigma f_i \bullet \delta^{18}O_{react\ i} + (\ln f_{NOx} + 1) \bullet \Sigma^{18}\varepsilon_{rxn\ i} \quad \text{(Open; 23)}$$

And

$$\delta^{17}O_{prod} = \Sigma f_i \bullet \delta^{17}O_{react\ i} + f_{NOx} \bullet \Sigma^{17}\varepsilon_{rxn\ i} \quad \text{(Closed; 24)}$$

$$\delta^{17}O_{prod} = \Sigma f_i \bullet \delta^{17}O_{react\ i} + (\ln f_{NOx} + 1) \bullet \Sigma^{17}\varepsilon_{rxn\ i} \quad \text{(Open; 25)}$$

These equations are less straightforward than the nitrogen case because f_i tends to be dominated by oxygen participating in the photo-oxidation rather than reflecting the oxygen isotopes in the initial NO_x emissions. This oxygen is mainly derived from O_3, O_2 and H_2O. Focusing on the $\Delta^{17}O$ of the reactants and products using isotope mass balance yielding:

$$\Delta^{17}O_{prod} = \Sigma f_i \bullet \Delta^{17}O_{react} + f_{NOx} \bullet \Sigma\Delta\varepsilon_{rxn} \quad (26)$$

where $\Delta\varepsilon_{rxn}$ is any MIF occurring during a NO_x-NO_y oxidation reactions. However, ozone formation is the only known tropospheric reaction that has a major MIF (Section "Isotopologues of tropospheric oxidants"), which only enters the NO_y cycle after the fact. Under this assumption then, $\Sigma\Delta\varepsilon_{rxn} = 0$, and since O_2 and H_2O both have $\Delta^{17}O \sim 0$‰, and that O_3 transfers the terminal O atom during oxidation reactions Eq. (26) reduces to.

$$\Delta^{17}O_{prod} = f_{O3} \bullet \Delta^{17}O_T \quad (27)$$

Where f_{O3} is the fraction of oxygen derived from O_3 and $\Delta^{17}O_T$ is the $\Delta^{17}O$ value of the terminal O atom of ozone that is equal to 1.5•bulk O_3 $\Delta^{17}O$. A higher $\Delta^{17}O$ measured in NO_{3atm}^- is thus interpreted as a higher O_3 oxidation potential.

To predict the $\Delta^{17}O$ of NO_{3atm}^- using this isotope mass balance approach requires assessing f_{O3} for the reactions (Fig. 1) that convert NO_x into NO_{3atm}^- (Michalski et al., 2003). First step is determining the $\Delta^{17}O$ in NO_2 from the basic NO_x cycle (R1–R3).

$$NO + O_3 \rightarrow NO_2 + O_2 \quad (R1)$$

$$NO_2 + h\nu\ (<420\ nm) \rightarrow NO + O \quad (R2)$$

$$O + O_2 + M \rightarrow O_3 + M \quad (R3)$$

Under mid-latitude daytime conditions, NO_2 is photolyzed approximately every 3 min so during peak daylight hours $f_{O3} = 1$ when other oxidants (HO_2, RO_2) are ignored and therefore $\Delta^{17}O_{NO2} = \Delta^{17}O_T$. Based on published tropospheric O_3 values this equates to $\Delta^{17}NO_2 \sim 39$z‰ (Vicars and Savarino, 2014). This agrees with NO_x-O_3 photochemical equilibrium experiments at high NO_x mixing ratios (ppm_v) (Michalski et al., 2014) and similar to the maximum value found in ambient NO_2 in Grenoble, France (Albertin et al., 2021). However, an explicit isotope kinetics model used to simulate the NO_x-O_3 photochemical equilibrium experimental data predicts a Δ^{17} $NO_2 \sim 45$‰ when NO_x is at ppb_v levels (Michalski et al., 2014). This discrepancy between observed NO_2 $\Delta^{17}O$ and experimental predictions maybe in part due to the fact that observed tropospheric O_3 $\Delta^{17}O$ values are lower than those in produced pressure and temperature O_3 formation experiments (Section "Isotopologues of tropospheric O_3").

NO oxidation is not exclusively by ozone, however, but can also occur through oxidation by peroxy radicals (Fig. 1, R 4). The majority of peroxy radicals are produced when radical species such as ·H, $\cdot CH_3$, and ·R (organic radical) generated by reactions with OH radicals, combine with atmospheric O_2 (R16) and the peroxy radicals subsequently oxidize NO (R4):

$$H\ (R\bullet) + O_2 \rightarrow HO_2\ (ROO) \quad (R16)$$

$$NO + HO_2\ (ROO\bullet) \rightarrow NO_2 + OH\ (RO\bullet) \quad (R4)$$

Yielding

$$\Delta^{17}O_{NO2} = \left(1 - f_{peroxy}\right) \bullet \Delta^{17}O_T = A \bullet \Delta^{17}O_T \quad (28)$$

since $f_{peroxy} + f_{O3} = 1$ (assuming all NO is oxidized by either O_3 or peroxy radicals). Setting $1\text{-}f_{peroxy} = A$ simplifies the equations and avoids variable symbols like α and β used previously (Michalski et al., 2003; Morin et al., 2009) that have other meanings in stable isotopes theory (See Section "Stable isotope abundance nomenclature, fractionations, and mass balance"). Peroxy radical oxidation of NO lowers the $\Delta^{17}NO_2$, which was shown by Albertin et al. to vary over the course of a day from 29.7‰ to 39.2‰ (Albertin et al., 2021).

Higher oxides of nitrogen, NO_3 and N_2O_5, are produced by additional oxidation by ozone (R6, R8). Again, the isotopic mass balance approximation can be used by assuming no MIF during the reactions. NO_3 radical obtain 2/3 of their O atoms from NO_2 and 1/3 from O_3 while N_2O_5 obtain 2/5 from NO_2 and 3/5 from NO_3:

$$NO_2 + O_3 \rightarrow NO_3 + O_2 \quad (R6)$$

$$\Delta^{17}O_{NO3} = 2/3\ A \bullet \Delta^{17}O_T + 1/3 \bullet \Delta^{17}O_T = [(2A + 1)/3] \bullet \Delta^{17}O_T \quad (29)$$

$$NO_2 + NO_3 \leftrightarrow N_2O_5 \quad (R8)$$

$$\Delta^{17}O_{N2O5} = 2/5\ A \bullet \Delta^{17}O_T + 3/5(2A + 1)/3 \bullet \Delta^{17}O_T = [(4A + 1)/5] \bullet \Delta^{17}O_T \quad (30)$$

In the final steps of nitric acid formation, two other oxygen sources enter into the equation, OH radicals and liquid water. The primary oxidation pathway for the production of nitric acid from NO_2 is through OH oxidation (R5) and where 2/3 O atoms in the product HNO_3 come from NO_2 and 1/3 from OH ($\Delta^{17}O = 0$). An important alternative pathway to form nitric acid is via the heterogeneous hydrolysis of N_2O_5 on wet aerosol surfaces (R9) and where 5/6 of the O atoms in the product HNO_3 come from N_2O_5 and 1/6 from H_2O. Finally, a minor but non-trivial pathway to nitric acid is through hydrogen abstraction from VOCs by nitrate radicals (R7) with all O atoms coming from the NO_3 radical. Using the assumption that $\Delta^{17}O$ values of both tropospheric water and for the EIE for the OH + H_2O isotope exchange reaction is 0‰ (Section "Isotopologues in the tropospheric HO_x cycle") then:

$$NO_2 + OH + M \rightarrow HNO_3 \quad \text{(R5)}$$

$$\Delta^{17}O_{R5} = 2/3 \bullet A \bullet \Delta^{17}O_T \quad (31)$$

$$NO_3 + VOC \rightarrow HNO_3 \quad \text{(R7)}$$

$$\Delta^{17}O_{R7} = (2A + 1)/3 \bullet \Delta^{17}O_T \quad (32)$$

$$N_2O_5 + H_2O + \text{surface} \rightarrow 2\ HNO_3 \quad \text{(R9)}$$

$$\Delta^{17}O_{R9} = 5/6(4A + 1)/5 \bullet \Delta^{17}O_T = (4A + 1)/6 \bullet \Delta^{17}O_T \quad (33)$$

For a A = 0.7 and a $\Delta^{17}O_T$ = 39‰ this yields $\Delta^{17}O_{R5}$ = 18.2‰, $\Delta^{17}O_{R7}$ = 31.2‰, and a $\Delta^{17}O_{R9}$ = 24.7‰, e.g. different $\Delta^{17}O$ values for the different oxidation pathways. The total $\Delta^{17}O$ value for HNO_3 is then:

$$\Delta^{17}O_{HNO3} = f_{R5} \bullet \Delta^{17}O_{R5} + f_{R7} \bullet \Delta^{17}O_{R7} + f_{R9} \bullet \Delta^{17}O_{R9} \quad (34)$$

Therefore, $\Delta^{17}O$ can be used to constrain the relative importance of NO oxidation by peroxy radicals (A = 1- f_{peroxy}) and the relative importance of the 3 HNO_3 production pathways: f_{R5}, f_{R7}, and f_{R9}. Given that R7 is typically a minor part of total HNO_3 production, the $\Delta^{17}O$ HNO_3 pathway effect is limited to about 22 ± 3‰ (at A = 0.7). Variations in A, on the other hand, have the potential to cause greater $\Delta^{17}O$ variation and should be observable in systems with high VOCs such as isoprene, which enhances RO_2 production. Conversely, when modeling NO_{3atm}^- $\Delta^{17}O$ using photochemical mechanisms (such as RACM or MCM), the models are used to calculate A, f_{R5}, f_{R7}, and f_{R9} from which the predicted $\Delta^{17}O$ is calculated and then to compared to the observed $\Delta^{17}O$ values.

This initial $\Delta^{17}O$ isotope mass balance approach proposed by Michalski et al. (2003) was subsequently amended to include additional reactions that become important in certain environments. In places where halogen chemistry becomes important such as the coastal polar region where halogens such as BrO mimic O_3 oxidization of NO, then A = 1- (f_{O3} + f_{BrO}). Also in these environments, $BrONO_2$ hydrolysis produces NO_{3atm}^- (Morin et al., 2009; Morin et al., 2008). Likewise, recent research has suggested heterogeneous hydrolysis of NO_3, NO_2, $RONO_2$ on aerosols and/or liquid water (fog, clouds, rain) may be important in highly polluted urban environments (Kim et al., 2023; Liu et al., 2019). For these, assuming no additional isotopic exchange with water, yields:

$$NO_3 \text{ hydrolysis}: \quad (2A + 1)/3 \bullet \Delta^{17}O_{1.5O3} \quad (35)$$

$$NO_2 \text{ hydrolysis}: \quad 2/3 \bullet A \bullet \Delta^{17}O_{1.5O3} \quad (36)$$

$$RONO_3 \text{ hydrolysis}: \quad 1/3 \bullet A \bullet \Delta^{17}O_{1.5O3} \quad (37)$$

$$XNO_3 \text{ hydrolysis (X = Br, Cl, or I)} \quad (2A + 1)/3 \bullet \Delta^{17}O_{1.5O3} \quad (38)$$

This $\Delta^{17}O$ mass balance model has been used to try and interpret $\Delta^{17}O$ in ambient NO_y collected from a range of environments.

Observations of $\delta^{18}O$ and $\Delta^{17}O$ of ambient NO_x and HONO

The direct measurement of NO_x $\delta^{18}O$ or $\Delta^{17}O$ in NO_x sources has received little attention because NO_x photochemical cycling is rapid (a few minutes) and any source signature is lost in the isotopic scrambling, but oxygen isotopes in ambient NO_x and HONO has been measured. Four studies have measured oxygen isotopes on NO_2 and several published collection/analysis techniques (Walters et al., 2018; Albertin et al., 2021; Blum et al., 2023; Zhou et al., 2022), suggesting more studies will be forthcoming. Felix and Elliot measured the $\delta^{18}O$ values of NO_2 collected by passive samplers inside a traffic tunnel and found an average of −12.6 ± 3.1‰ while outside the tunnel the values ranged from −8.4 to +7.8‰ (Felix and Elliott, 2014). They attributed this to negative $\delta^{18}O$ in tail pipe NO_2 (tunnel) mixing with photo equilibrated NO_2 (outside), while others suggested it was an artifact because the passive sampling technique impacts the oxygen isotopes (Dahal and Hastings, 2016). Walters et al. measured the $\delta^{18}O$ of NO_2 in a rural site finding a range between ~ +40 and +110‰, with daytime values (86.5 ± 14.1‰) being significantly higher than nighttime values (56.3 ± 7.1‰). This was attributed to isotopic photo-equilibrium with O_3 during the daytime and nighttime NO_x emissions that cannot photo-equilibrate in darkness (Walters et al., 2018). Albertin et al. first measured both $\Delta^{17}O$ and $\delta^{18}O$ of NO_2 in a study during a single day of sampling collected at three-hour intervals and also found a diurnal difference as well significant daytime variation (Albertin et al., 2021). Daytime NO_2 $\Delta^{17}O$ values varied between a low of 29.7‰ and peaked in the late morning at 39.2‰ before decreasing at night to 20.5 ± 0.3‰. There was a strong correlation between NO_2 $\delta^{18}O$ and $\Delta^{17}O$ with an R^2 = 0.86. The daytime $\Delta^{17}O$ and $\delta^{18}O$ variability was attributed to changes in the proportion of NO oxidized by O_3 relative RO_2, while the night-time decrease was due to isotopic dilution by freshly emitted NO that produce NO_2 that has yet to photo-equilibrate. This is because during the night, any NO emitted can still undergo oxidation chemistry when O_3 is present and subsequent isotope exchange with higher N oxides such as via EX. 1 and R8. The first measurements of the $\delta^{18}O$ of HONO have recently been reported (Chai et al., 2019). HONO collected in western US wildfire plumes had a low $\delta^{18}O$ in unaged plumes of 9.8‰ and a high in aged plumes of 78‰. The isotopes suggested that 85% to 95% of HONO production was NO_2-to-HONO heterogeneous reactions and only 5% to 15% was from the OH + NO reaction and was used to constrain the ozone and peroxy radicals branching ratio (R1, R3).

Observations of $\Delta^{17}O$ in NO_{3atm}^-

The number of studies utilizing $\Delta^{17}O$ to understand NO_y chemistry has grown rapidly over the past decade. An analysis of over 1000 published NO_{3atm}^- $\Delta^{17}O$ values yielded a mean of 25.9‰ with 1σ standard deviation of 5.5‰ (Fig. 9). The few maximum outliers near +40‰ are aerosols collected from Antarctica/South Pole and the cluster of outlier minimums at 10 ± 5‰ were NO_3^- extracted from total suspended particles collected at Mt. Lulin, Taiwan. Both these extremes are consistent with the global NO_{3atm}^- $\Delta^{17}O$ modeling using GEOS-Chem (Alexander et al., 2009a; Alexander et al., 2020). The high valued Antarctica/SP aerosols were collected during the months of August and September (Savarino et al., 2007; Walters et al., 2019) when Alexander et al.'s model predicts $\Delta^{17}O$ ~40‰ over Antarctica. Other high values above the 3rd quartile (+34 ± 5‰) are from megacities in China during severe haze events when N_2O_5 hydrolysis plays an important role in NO_{3atm}^- production (Fan et al., 2023; Wang et al., 2023; Yin et al., 2022; Zhang et al., 2022). The low $\Delta^{17}O$ values from Mt. Lulin (Guha et al., 2017) were primarily from samples collected in June–September when the GEOS-Chem model predicts $\Delta^{17}O$ to be ~10‰ (see Fig. 13) over southeast Asia and the islands of Oceania. These low $\Delta^{17}O$ predictions are due to VOC emissions from tropical rainforests causing a decrease in the A factor via increased peroxy radical oxidation of NO (R4). Back trajectories confirmed that many of the sampling days corresponded with transport to Taiwan from the low $\Delta^{17}O$ regions (Guha et al., 2017). The mean $\Delta^{17}O$ value for all studies may be biased high because the data is disproportionately from large urban areas in China, the US, and Europe and polar regions, where $\Delta^{17}O$ values in NO_{3atm}^- are expected to be high relative to the total planetary boundary layer (Alexander et al., 2020).

One consistent observation between long-term studies (~1 year) is the $\Delta^{17}O$ seasonal pattern (Guha et al., 2017; Huang et al., 2020; Kaiser et al., 2007; Kim et al., 2023; Michalski et al., 2003; Wang et al., 2019). $\Delta^{17}O$ values in NO_{3atm}^- peak in winter months and decline to their minimum values in summer (Fig. 9). The working hypothesis to explain this observation is a shift in chemistry related to sunlight and temperature. Longer nights tend to favor the production of nitrate radical and N_2O_5, which are photolyzed during the daytime. In addition, cooler temperatures favor the N_2O_5 product in the R8 equilibrium. Therefore, the winter months or more conducive to the production of nitric acid by that heterogeneous hydrolysis pathway (Chang et al., 2018; Dentener and Crutzen, 1993; Michalski et al., 2003). In contrast during the summer, sunlight produces more OH radicals and peroxy radicals, which decreases the A factor and enhances nitric acid production via the OH pathway (Alexander et al., 2009a; Alexander et al., 2020; Michalski et al., 2003).

High temporal/spatial resolution NO_{3atm}^- sampling has shown that $\Delta^{17}O$ has the ability to trace changes NO_x oxidation chemistry, not only at the seasonal scale, but at the at the hourly scale as well. Nitrate in rainwater collected from the same storm system collected at multiple sites within the city of Tucson, USA had a large spatial $\Delta^{17}O$ variation of 22.1 to 30.6‰ (Riha et al., 2014). Similarly, high temporal sampling of the same storms at a single site in West Virginia, USA showed that rainwater $\Delta^{17}O$ can vary by 10‰ over the course of a single event suggesting evolving chemistry as wet deposition removes pollutants from the atmosphere (Rose et al., 2019). NO_3^- extracted from $PM_{2.5}$ collected roughly every 3 h for 2 weeks during an extreme haze event in Nanjing, China (Zhang et al., 2022) showed $\Delta^{17}O$ varying by 15‰ (Fig. 10). The temporal changes appeared to be related to extreme changes in O_3 concentrations, which dropped to near zero during the night, likely due to O_3 loss on particle surfaces.

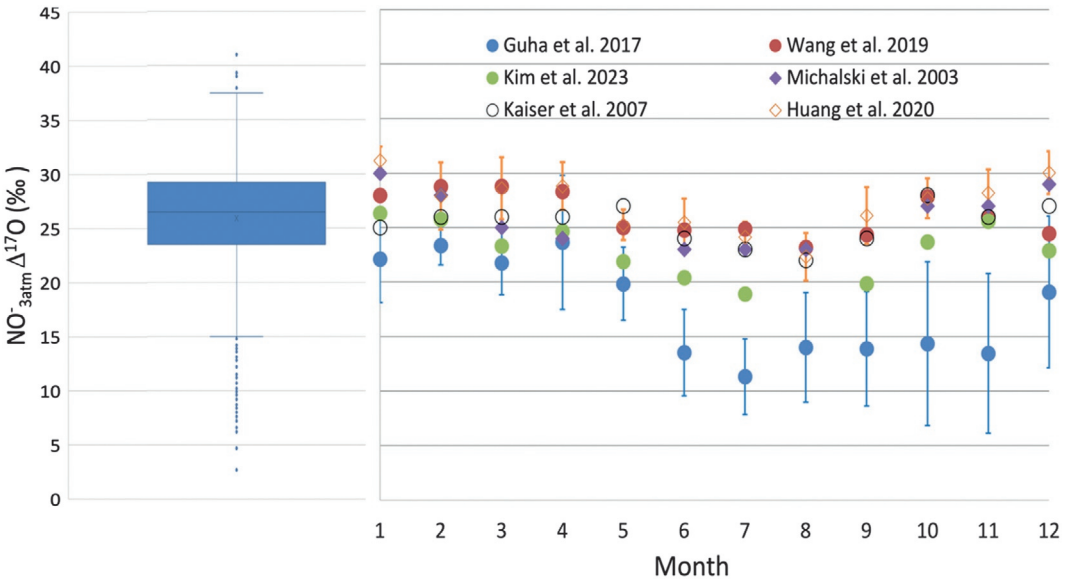

Fig. 9 A box and whisker plot of $\Delta^{17}O$ in NO_{3atm}^- collected in the troposphere. The middle line of the box is the median, the X represents the mean, bottom of the box is the 1st quartile the top is median of the 3rd quartile. The whiskers extend capture minimum value and maximum values and data points are considered statistical outliers. On the right is the seasonal change in $\Delta^{17}O$ of NO_{3atm}^- for select northern hemisphere, mid-latitude sampling sites. The NO_{3atm}^- types are aerosols (Michalski et al., 2003; Wang et al., 2019), rainwater (Guha et al., 2017; Kaiser et al., 2007; Huang et al., 2020), and gas phase HNO_3 (Kim et al., 2023). Error bars on Guha et al. and Huang et al. are the measured $\Delta^{17}O$ variation within a given month with the former collection period spanning a year and the latter 3 years.

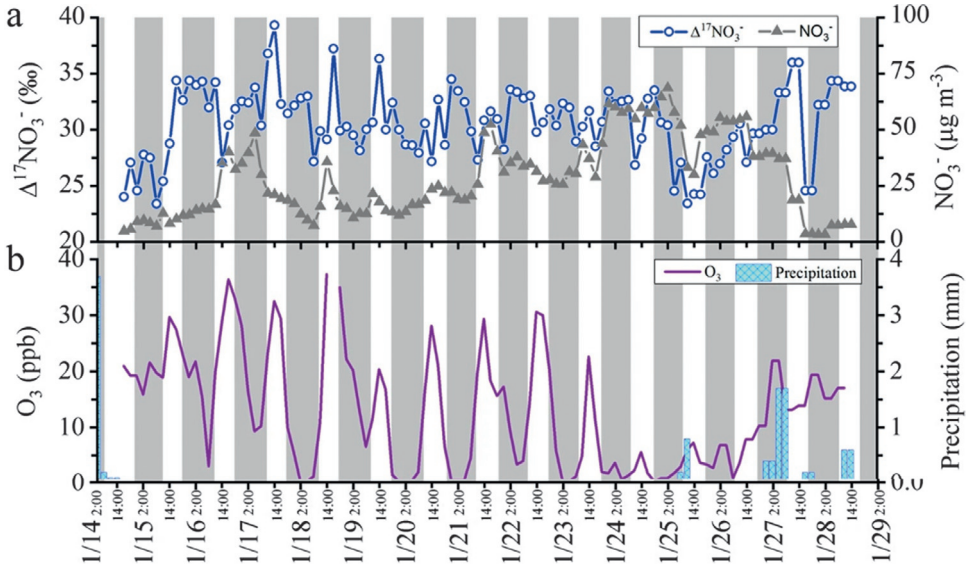

Fig. 10 The $\Delta^{17}O$ of NO_3^- in $PM_{2.5}$ collected in late January (2015) in Nanjing, China during an extreme haze event. Over the course of the event the $PM_{2.5}$ increased from 50 to 250 μg/m^3 over the two-week period along with pNO_3^- (upper panel). Low $\Delta^{17}O$ were associated with low O_3 concentrations and wet deposition of PM and gases due to rain occurring (lower panel) at the end of the event. Adapted from Zhang YL., Zhang W, Fan MY, Li J, Fang H, Cao F, Lin YC, Wilkins BP, Liu X, Bao M, Hong Y, and Michalski G (2022) A diurnal story of $\Delta^{17}O$ NO_3^- in urban Nanjing and its implication for nitrate aerosol formation. *npj Climate and Atmospheric Science* 5(1). https://doi.org/10.1038/s41612-022-00273-3.

Also, a significant drop in $\Delta^{17}O$ (~10‰) occurred just after rain cleansed the atmosphere, again tracing the change in chemistry driven by wet deposition removal of pollutants from the boundary layer. Recent data from Kim et al. has shown that the shifts in NO_x oxidation pathways also is evident in the phase of $NO_{3\bar{atm}}$. Analyzing samples of HNO_3(g) and pNO_3^- co-collected from three US EPA Clean Air Status and Trends Network (CASTNET) sites in the northeastern US yielded statistically significant differences between gas phase HNO_3 and pNO_3^- at all 3 sites (Kim et al., 2023). The HNO_3 had a $\Delta^{17}O$ mean of 22.8 ± 3.6‰ while the pNO_3^- was about 5‰ higher at 27.1 ± 3.8‰. This would be consistent with gas phase OH reaction (R5) generating lower $\Delta^{17}O$ values in gas HNO_3 relative to the direct uptake of N_2O_5 on particle surface that would produce higher $\Delta^{17}O$ values (R9, Eq. 33). Once in the particle phase it is unlikely that HNO_3 could be volatized from pNO_3^- given the extremely high Henry's law coefficient for HNO_3 and that HCl will volatilize before HNO_3. This suggest that HNO_3(g) is unequilibrated with the particle phase at these CASTNET sites. This may be different in environments where NH_4NO_3 is the main chemical composition of pNO_3^- and phase equilibrium is more readily achieved and equitable (Morino et al., 2006).

Observations of $\delta^{18}O$ in $NO_{3\bar{atm}}$

The $\delta^{18}O$ values of $NO_{3\bar{atm}}$ are usually highly correlated with the $\delta^{17}O$ and $\Delta^{17}O$ values (Fig. 11). While the slopes slightly vary between study sites, there is a typical slope $\delta^{17}O/\delta^{18}O$ of about 0.85 ± 10 in the dual isotope ratio plot of NO_3^- (Fig. 12), with high correlation coefficients (>0.93). Since excess ^{17}O is derived solely from O_3 oxidation transfer reactions, this strong correlation suggests that the $\delta^{18}O$ in $NO_{3\bar{atm}}$ must also be largely controlled by O_3's $\delta^{18}O$ composition, since the $\delta^{18}O$ T and P dependence can cause a ±20‰ $\delta^{18}O$ variation under tropospheric conditions. However, it is more likely to be true that this strong correlation is the result two distant end members in an isotope mixing line, one being O_3, and the other oxygen derived from compounds laying on the TFL (Fig. 11, left). There are several interpretations of the intercept at the TFL. The first is that the $\delta^{18}O$ of $NO_{3\bar{atm}}$ is a mixture between the $\delta^{18}O$ of O_3 and average tropospheric H_2O. Alternatively, since NO oxidation can incorporate O_2 (R4) and HNO_3 formation incorporates OH (R5), the mixing line could be between O_3 and a ~ 50:50 mixture of O_2 and OH derived oxygen (Fig. 12 left). Lastly, an equitable mixture of all 3 mass-dependent oxygen sources would have a $\delta^{18}O$ ~–10‰, similar to the TFL intercept (Fig. 11). The difficulty in interpreting the TFL intercept is that extrapolating the slope over ~80‰ means that even a small uncertainty in the slope changes the TFL intercept significantly. A convenient visualization to understand the ^{17}O vs. ^{18}O relationship is an $\Delta^{17}O$ vs. $\delta^{18}O$ scatter plot (Fig. 11, right). Michalski et al. first showed that such a plot was useful for assessing mixing between photochemical and microbial derived NO_3^- in watersheds (Michalski et al., 2004) but this is true for any mixture between non-zero and a zero $\Delta^{17}O$ reservoirs. In other words, the y-intercept (when $x = \Delta^{17}O = 0$) represents the $\delta^{18}O$ of the total NO_x oxidation process, both the $\delta^{18}O$ of the source (s) and the $\delta^{18}O$ alteration via mass-dependent isotope fractionations. Now differences in the intercepts between the two sets of studies is clear. The interpretation here would be that the HNO_3 and pNO_3^- in the CASTNET samples (Kim et al., 2023) were more influenced by O_2 oxidation whereas the rain NO_3^- samples have a greater contribution of H_2O oxygen (Guha et al., 2017; Huang et al., 2020). That the NO_3^- in rain has a greater contribution of H_2O compared to pNO_3^- and HNO_3(g) is intriguing because rain NO_3^- is derived either from washout of boundary layer pNO_3^- and

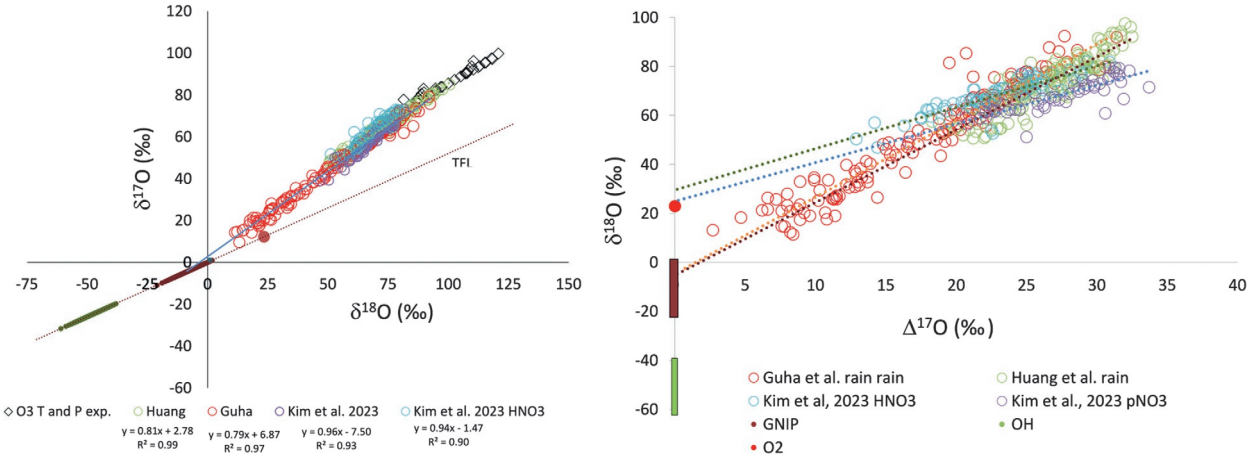

Fig. 11 Dual oxygen isotope ratio plot of NO_{3atm}^- (left) from 3 select studies (Guha et al., 2017; Huang et al., 2020; Kim et al., 2023). The $\delta\ ^{17}O/\delta\ ^{18}O$ ratio is high (0.8) with very high correlation coefficients ($R^2 > 95$), similar to other studies. The line between troposphere O_3 (based on T and P experiments) and the intercept at the TFL represents a two end-member isotope mixing line. The Guha et al. intercept could be interpreted as a mixture between tropospheric O_3 and either tropospheric H_2O (maroon TFL array), or a 50:50 mixture of OH (green TFL array) and O_2 (TFL red circle) derived oxygen, or some combination of the two. A $\Delta^{17}O$ vs $\delta^{18}O$ plot of NO_{3atm}^- from the same 3 studies (right). The best fit line extends through the $\delta^{18}O$ values of the non-O_3 oxidants. The spread in $\delta^{18}O$ values on the can be the result of both $\delta^{18}O$ variation in the compounds (mainly H_2O) and mass-dependent isotope effects occurring during NO_x oxidation into NO_{3atm}^-.

HNO_3 or rainout of cloud water where dissolved NO_3^- is presumably from dissolution of boundary layer cloud condensation nuclei during cloud formation. This means there should be little difference in the between the $\delta^{18}O$ of all phases of NO_{3atm}^-. The observed lower $\delta^{18}O$ intercept for rain NO_3^- could only be explain by an unaccounted-for aqueous phase reaction that either produces NO_3^- or induces some isotopic exchange between NO_y and water.

Modeling isotopologues of NO_{3atm}^-

Because NO_y isotopologue abundance variations at any point in time are a complex function of NO_x emission abundances, their mixing in the atmosphere during transport, and the four mass-dependent isotope effects and O_3 MIF altering the mixture during transport, computer models are becoming increasingly important for understanding this complexity. Modeling highly reactive isotopologue variations has two general forms: Mass balance mixing models and explicit mechanistic models. Each has different levels of sophistication, advantages, and disadvantages.

Isotope mass balance mixing models for $\delta^{15}N$, $\delta^{18}O$, and $\Delta^{17}O$

Isotope mass balance mixing models (Section "Isotope mass balance") assume that isotopologues are acting as conservative tracers in the atmosphere and the time and/or space variations in $\delta^{15}N$, $\delta^{18}O$, and $\Delta^{17}O$ values is a result of the mixing between two or more reservoirs of the same compound. For example, variations of $\delta^{15}N$ in NO_{3atm}^- has been explained by mixing of NO_x sources with different $\delta^{15}N$ values, such as coal and vehicles (Elliott et al., 2007). Some isotope mass balance mixing models have incorporated Bayesian statistics (Parnell et al., 2013) using prior knowledge about source $\delta^{15}N$ values to use $\delta^{15}NO_{3atm}^-$ to help constrain NO_x sources (Tian et al., 2021; Wang et al., 2017; Xiao et al., 2020). These models typically ignore any isotope effect occurring during the photochemical oxidation of NO_x, although some have incorporated a single oxidation enrichment factor to account for the isotope fractionation (Song et al., 2021). Such models may or may not be accurate depending on the sample collection conditions. For short timescales sampling, such as hourly, the $\delta^{15}N$ (and $\delta^{18}O$, $\Delta^{17}O$) is likely to be significantly influence by the immediate conditions (Albertin et al., 2021; Walters et al., 2018) such as pollutant load and sunlight intensity (or lack thereof). Extended collection periods (days to weeks) would modulate the temporal effects and would better represent a $\delta^{15}NO_{3atm}^-$ that is a function of NO_x source mixing plus single isotope fractionation factor for that time period. In cases where the majority of NOx (>90%) is oxidized into $^{15}NO_{3atm}^-$ quickly, such as plumes or urban areas under a severe inversion layer and minimal advection, an isotope mass balance of all NOx sources is likely to be close to the $\delta^{15}NO_{3atm}^-$.

The role of the temporal and spatial variation of $\delta^{15}NO_x$ emissions and the effect of mixing during boundary layer transport was recently modeled using the Community Multi-scale Air Quality (CMAQ) model (Fang and Michalski, 2022). That model ($_{iN}$CMAQ) used the US Environmental Protection Agency's (US-EPA) 2002 National Emission Inventory (NEI) to estimate hourly NO_x emissions at 12 km grid resolution for the Midwestern US (Fig. 12). Based on the fraction of NO_x from each source in a given grid and the $\delta^{15}NO_x$ values for different sources (Section "Isotopes of N in precursor gases NO_x and NH_3"), the time and space dependent $\delta^{15}NO_x$ emissions were simulated hourly for 1 year (2002). Theses emissions were then mixed by boundary layer transport via meteorology derived from the Weather Research and Forecasting (WRF) model. The results show that transport plays

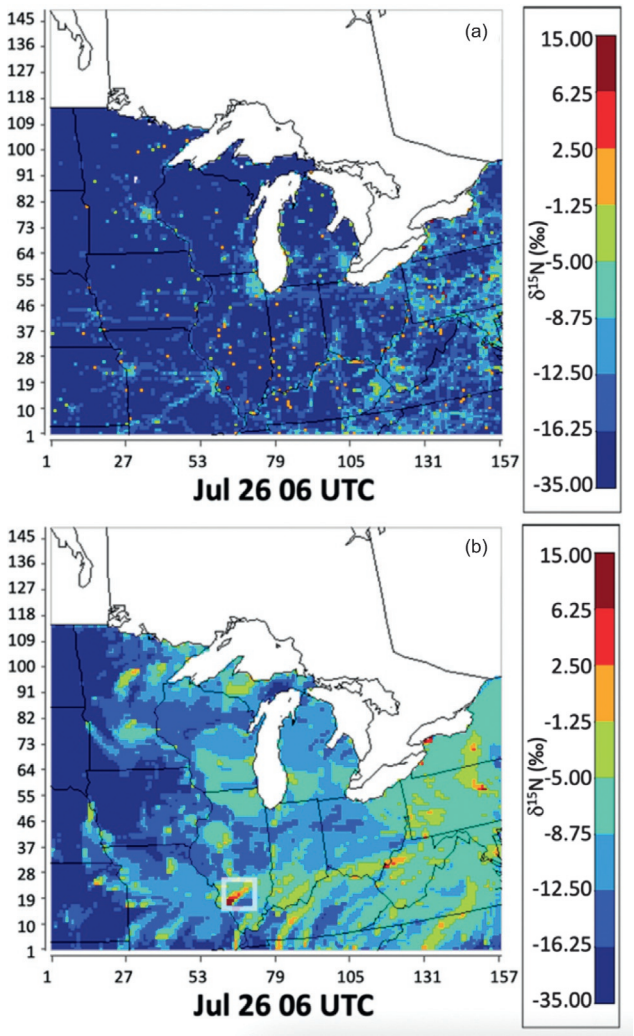

Fig. 12 Upper panel (a) is the $\delta\ ^{15}NO_x$ of emissions for the Midwestern USA at 12 km^2 grid resolution based on emission data from the US-EPA NEI (2002). The lower panel (b) is the $\delta\ ^{15}NO_x$ when boundary layer mixing is added to CMAQ using WRF derived meteorology. Mixing homogenizes the gridded emissions (a) and $\delta\ ^{15}NO_x$ plumes from high emitting EGUs are clearly visible (white box). From Fang H and Michalski G (2022) Assessing the roles emission sources and atmospheric processes play in simulating $\delta^{15}N$ of atmospheric NO_x and NO_3^- using CMAQ (version 5.2.1) and SMOKE (version 4.6). *Geoscientific Model Development* 15(10): 4239–4258. https://doi.org/10.5194/gmd-15-4239-2022.

an important role for the $\delta^{15}NO_x$ at any place and time. Specifically, it shows how large point sources, such as EGU's without NO_x reduction technology, can influence the regional $\delta^{15}NO_x$ and that this influence is not evenly distributed, rather $\delta^{15}N$ plumes follow prevailing winds and the storm transport dynamics typical of regional air flow (Fig. 12). Many observational studies have used the HYSPLIT model (Stein et al., 2015) to calculate back trajectories in order try in detect this transport effect (Buda and DeWalle, 2009; Elliott et al., 2019; Michalski et al., 2022). The goals of such models are twofold. First, it can be used to assess whether the model is correctly capturing the observed $\delta^{15}N$ in the atmosphere. If not, then the second application would be to assume that the difference between the observation and the model is due to incorrect NO_x emissions estimates by the NEI, which means this $\delta^{15}NO_x$ model could be used as a new tool for NO_x source verification. Of course, this ignores the photochemical isotope effects during NO_x to NO_y conversion, which are important, and are being incorporated in future versions of $_{i\mathrm{N}}$CMAQ (Fang and Michalski, 2022).

Isotope mass balance mixing models have also been used to simulate $\Delta^{17}O$ by assessing the fraction of oxidation pathways during the oxidation of NO_x to NO_y and assumptions about the $\Delta^{17}O$ value of those pathways (Section "Oxygen isotopes fractionations during the production of NO_y and tropospheric observations"). These oxidation pathway fractions have been calculated using either simple photochemical box models, using known chemical mechanisms, or using chemical mechanisms imbedded in 3-D chemical transport models. Michalski et al. used the photochemical box model of Yvon et al. (Yvon et al., 1996) to calculate the A factor (Eq. 18) and the f_{R5}, f_{R7}, and f_{R9} (Eq. 34) and assumed an O_3 bulk $\Delta^{17}O$ of 35‰ based P and T experiments but assumed all O atoms transfer, which is equivalent to a bulk O_3 of $\Delta^{17}O$ 23‰ (similar to obervations by Johnston and Theimens) and a terminal atom transfer. This model matched observed $\Delta^{17}O$ in pNO_3^- fairly well, including capturing the seasonal

$\Delta^{17}O$ trend. Subsequent models have incorporated additional pathways (Eqs. 34–37) and used different mechanisms (Michalski et al., 2011; Morin et al., 2011) and have reproduced observed NO_{3atm}^- $\Delta^{17}O$ values and trends fairly accurately. The $\Delta^{17}O$ mass balance approach was incorporated into the 3-D chemical transport model GEOS-Chem (Alexander et al., 2009a; Alexander et al., 2020) that predicted NO_{3atm}^- $\Delta^{17}O$ values globally as a function of season (Fig. 13). The model accurately predicts the sunlight effect, where long hours of darkness enhances HNO_3 production via the N_2O_5 and NO_3 pathways (Dentener and Crutzen, 1993) and increase the A factor due to fewer radicals being produced under low sunlight conditions (Alexander et al., 2009a; Alexander et al., 2020). This results in maximum NO_{3atm}^- $\Delta^{17}O$ values during the winter months in both the northern hemisphere (DJF) and southern hemisphere (JJA). Conversely, extended sunlight hours during the summer months increase HO_2/RO_2 production, lowering the A factor and greater OH production enhancing the R5 pathway of HNO_3 production resulting in $\Delta^{17}O$ minimums in the tropics. This simulated seasonal $\Delta^{17}O$ oscillation captures the observed trends very well (Fig. 9) but a comparison of $\Delta^{17}O$ values from 14 observational data sets with those predicted by GEOS-Chem predicted values yields a correlation coefficient of only $R^2 = 0.51$. The model also predicts within hemisphere NO_{3atm}^- $\Delta^{17}O$ spatial variations, where low values tend to be located over tropical rain forests (Fig. 13). This is attributed to enhanced RO_2 oxidation of NO (R4), which lowers the A factor, over rainforests due to high emission rates biogenic VOC's such as isoprene.

Isotope mass balance models to predict the $\delta^{18}O$ in NO_{3atm}^- have received less attention due to additional complexity of source ^{18}O and the lack of knowledge of mass-dependent isotope effects occurring during oxidation of NO_x into NO_y. The $\delta^{18}O$ value of oxidant sources introduces a number of uncertainties that must be accounted for in any modeling attempt. Tropospheric O_3 $\delta^{18}O$ values should vary between 80‰ and 108‰ for temperatures and pressures of the troposphere (Michalski et al., 2011), which is close to those observed in tropospheric O_3 (Fig. 4). Similarly tropospheric water $\delta^{18}O$ varies significantly in space and time depending on the water vapor sources region, ambient temperatures, and distillation effects occurring during precipitation that are a function of transport distance and elevation (Gat, 1996). For example, the average $\delta^{18}O$ of precipitation over the continental US varies by ~20‰ based on tap water analysis (Bowen and Revenaugh, 2003) and these absolute values change with season. In addition, there is a temperature dependent isotope portioning between the gas and liquid phase, with liquid H_2O having higher $\delta^{18}O$ values relative to the condensed phase (clouds, fog, rain). This means that the water used in R5 via the OH-H_2O EIE (vapor) and in R8 (liquid) would have different $\delta^{18}O$ values for the same air mass. Based on these assumptions an isotope mass balance

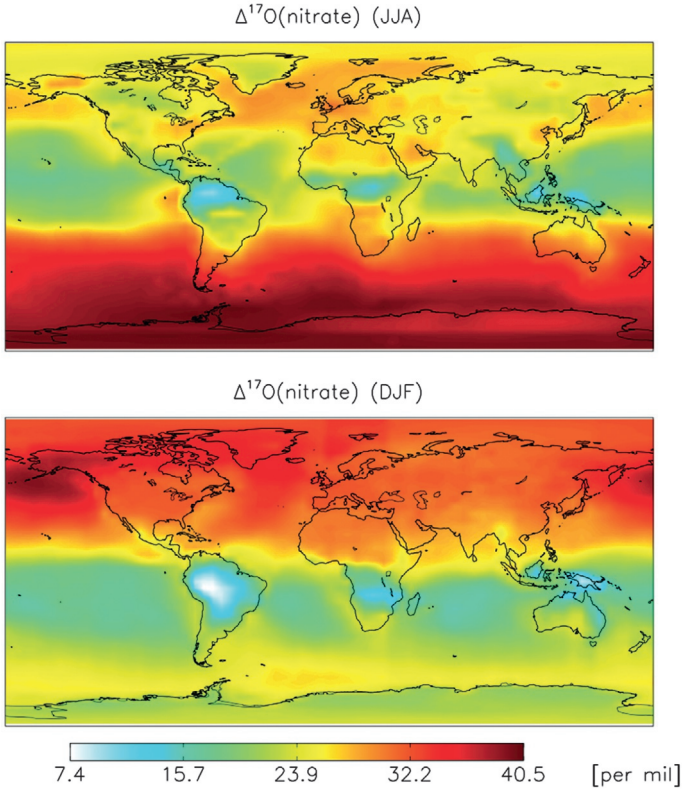

Fig. 13 $\Delta^{17}O$ enabled GEOS-Chem model of NO_{3atm}^- for summer (JJA) and winter (DJF). The hemispheric differences between seasons highlights the effect of sunlight hours while within hemisphere variations is driven by regional emissions, in particular VOC's emitted by tropical rain forests. From Alexander B, Hastings MG, Allman DJ, Dachs J, Thornton JA, and Kunasek SA (2009a) Quantifying atmospheric nitrate formation pathways based on a global model of the oxygen isotopic composition ($\Delta^{17}O$) of atmospheric nitrate. *Atmospheric Chemistry and Physics* 9(14): 5043–5056. https://doi.org/10.5194/acp-9-5043-2009; Alexander B, Park RJ, Jacob DJ, and Gong SL (2009b) Transition metal-catalyzed oxidation of atmospheric sulfur: Global implications for the sulfur budget. *Journal of Geophysical Research-Atmospheres* 114: https://doi.org/10.1029/2008jd010486.

model predicted tropospheric $NO_{3\bar{atm}}$ over the continental US should range between 26 and 50‰ (Michalski et al., 2011) significantly lower than observations (Fig. 9). The lower values predicted in the model were largely a function of the assumed $\delta^{18}O$ of OH (−50 to −80‰) that were a function of both water vapor $\delta^{18}O$ and the EIE $\varepsilon_{OH/H2O}$ of −40‰. The model also ignored the isotope fractionation via EIE, KIE, VPIE, and PHIFE which was a serious limitation.

Explicit mechanistic models for simulating $\delta^{15}N$, $\delta^{18}O$, and $\Delta^{17}O$

Explicit mechanistic models use the isotope fractionation factors occurring during EIE, KIE, VPIE, and PHIFE in chemical kinetic and 3-D chemical transport models to determine $\delta^{15}N$, $\delta^{18}O$, and $\Delta^{17}O$ values as a function of time and/or space. Some of these models have been used to explain experimental data, which is in turn used for interpreting in situ observations. For example, $\delta^{18}O$ and $\delta^{17}O$ data from O_3 synthesis experiments were used to derive O_3 isotopologue and isotopomer rate constants (i.e., α values) (Janssen et al., 1999, 2003; Janssen et al., 2001) that were then used to predict tropospheric O_3 $\delta^{18}O$ and $\Delta^{17}O$ values. These same rate constants were used to interpret $\delta^{18}O$ and $\Delta^{17}O$ in NO_2 produced in a NO_x-O_3 photochemical equilibrium experiment (Michalski et al., 2014) that helped to constrain recent NO_2 isotopologue observations (Albertin et al., 2021; Walters et al., 2018). Lyons used 70-reactions in a 1-D transport model assuming the all the isotope effects were through 11 isotopes exchange reactions among short lived radical species (Lyons, 2001) and predicted $NO_{3\bar{atm}}$ $\Delta^{17}O$ close to the measurements of Michalski et al. (2003). These types of studies are closed system, equilibrium simulations where the system reaches an isotopic steady state. A time dependent model of NO_y photochemistry, called $_{i\mathrm{N}}$RACM (Fang et al., 2021) incorporated 16 different ^{15}N isotopologues and 96 isotope fractionation factors (EIE, KIE and PHIFE) into the Regional Atmospheric Chemistry Mechanism RACM (Fang et al., 2021; Stockwell et al., 1997). This model showed the importance of day and night chemistry where LCIE is important during the day and NO_y EIE are more important at night (Fig. 7), suggesting a day-to-night difference in the $\delta^{15}N$ values of NO_y compounds (Albertin et al., 2021; Walters et al., 2018). The model reproduced an observational dataset from Tucson (USA) including the seasonal trend with fair accuracy with the deviations attributed to possible NO_x source changes with the seasons (Fang et al., 2021). The model also showed the importance of NO_x oxidation progress (i.e., the fraction of NO_x remaining) has on the resulting $NO_{3\bar{atm}}$ $\delta^{15}N$ values highlighting that simple isotope mass balance models are insufficient for understanding $NO_{3\bar{atm}}$ $\delta^{15}N$ dynamics.

Future explorations of NO_y isotopologue systematics

While there have been great strides in understanding stable isotope variations in tropospheric NO_y compounds and their relevance to identifying NO_x sources and tracing oxidation chemistry over the past two decades it is safe to say there is still much to learn. Future investigations can be broadly classified in three areas of research: in situ measurements, laboratory experimentation, and modeling, from the molecular scale to global 3D chemical transport modeling.

Future in situ NO_y isotopologue measurements

There is much to be gained from continuing to conduct in situ measurements of isotopologues of NO_y, especially examining their spatial and temporal variability, the covariation of different NO_y compounds and other variables in the same system, and NO_x emission sources. The spatial variability of NO_y around the planet remains largely unexplored. Most existing measurements have been relegated to urban and suburban environments in the US, Europe, and East Asia. Only a handful of studies have been conducted in the open ocean and even fewer in unique biomes such as deciduous or evergreen forests, semi-arid and arid ecosystems, tropical rainforests, or tundra ecosystems. There are also relatively few studies in the southern hemisphere other than Antarctica. In particular the near absence of data from Africa and South America is a glaring shortcoming. There are unique opportunities to collect NO_y in developing countries that currently have severe air pollution issues, such as India, Pakistan, and southern Asia, as a baseline to compare to NO_y in the future and see how air quality remediation affects NOy isotopologues over time. Perhaps even more importantly for understanding NO_y isotopologue variations is sampling at high temporal resolution since NO_y chemistry evolves on hourly timescales. Of particular interest would be detailed investigations of the differences between daytime and night-time NO_y isotope compositions, especially post rainfall sampling that could provide insight into how isotopologue compositions evolve going from clean to polluted conditions. Likewise, additional sampling periods that extend to a single year or beyond at different locations would be informative. There would also be great utility in combining spatial and temporal investigations by taking advantage of existing sampling infrastructure such as the NADP network in the USA. A year-long dataset of $\delta^{15}N$, $\delta^{18}O$, and $\Delta^{17}O$ in $NO_{3\bar{atm}}$ from each site in the NADP network would be invaluable for testing 3-D isotope enabled chemical transport models predictions and their mechanistic assumptions. Ideally, spatial and temporal sampling should be guided by existing hypothesis generated by current modeling results. For example, the low $\Delta^{17}O$ values of $NO_{3\bar{atm}}$ over tropical regions predicted by GEOS-Chem have yet to be observed. Likewise, the low seasonal amplitude of $NO_{3\bar{atm}}$ $\Delta^{17}O$ values predicted to occur in equatorial regions has yet to be investigated. Such in situ measurement investigations should strive to measure isotopes in as many NO_y compounds as feasible. For example, there has yet to be a study that has simultaneously measured NO_x, pNO_3^-, HNO_3, and rain NO_3^- for $\delta^{15}N$, $\delta^{18}O$, $\Delta^{17}O$, and O_3 $\Delta^{17}O$ and assessed how these values are related to one another. The measurement of heretofore unmeasured NO_y compounds such as PAN and organic nitrates will surely help in our understanding of how isotopes partition during NO_y chemistry. In addition to the collection and isotopic analysis of NO_y from various systems, simultaneous

measurements other variables such as temperature, relative humidity, wind direction and speed, and trace gases such as ozone, carbon monoxide, and VOCs would be of great utility for linking the photochemistry to the NO_y isotopologue variations. To this end researchers investigating NO_y isotopologues should become engaged with large sampling campaigns conducted by US agencies such as the DOE, EPA, NASA, and NOAA or their counterparts and Europe, Asia and Oceania. There is also much to be learned from the direct collection of NO_x from various sources including those that have yet to be measured such as ships, trains, aircraft, and industrial sources such as refineries, and ethanol, fertilizer and nitric acid plants. Measurements of oxygen isotopes in all NO_x sources may also prove useful for understanding diurnal variation in NO_{3atm}^- $\delta^{18}O$ and $\Delta^{17}O$ values.

Experimental investigations of NO_y isotopologue systematics

In order to fully understand the observed variation of isotopologues in NO_y there must be a concerted effort to conduct experimental investigation using photochemical chambers. For example, most of the assumptions in the $\Delta^{17}O$ mass balance model for NO_{3atm}^- have yet to be tested experimentally, such as does only one oxygen atom from water become incorporated into HNO_3 during the heterogeneous hydrolysis reaction or does the OH radical fully equilibrate with water vapor in the troposphere. Given the low mixing ratios of NO_x or other NO_y precursors in the troposphere, experiments investigating the isotopologue systematics would best be conducted in large chambers where reactant concentrations could be kept close to those in the troposphere and where wall effects are kept to a minimum. To date experimental investigations typically have focused on one isotopologue, either ^{15}N or ^{17}O, and future experiments that measure multiple compounds and multiple isotopes from the same system would be very valuable for understanding what is happening in the troposphere.

Computational analysis of NO_y isotopologue

Finally, there is much to accomplish computationally, from the molecular to the global scale for understanding the variation of isotopologues in NO_y. At the molecular scale using quantum chemistry techniques for determining isotope fractionation factors has much potential. This could be for testing whether quantum mechanical predictions match the experimental values or predicting isotope fractionation factors for reactions that are too difficult to measure experimentally. These isotope fractionation factors are required for in order for explicit isotope kinetics models to be developed and be accurate. Explicit isotope mechanistic box modeling can be quite insightful and help guide in situ measurements decisions. Exploring current ^{15}N model simulations and developing new explicit $^{18}O/^{17}O$ models will be useful for interpreting both in situ and experimental results. There is clearly a need to develop regional isotope enabled high resolution 3D chemical transport models. This is because of the high reactivity of NO_y, and the isotope effects associated with this reactivity will be highly sensitive the grid scale of any chemical transport model. For example, the isotopologue chemistry occurring in a plume, either from electrical generation units or biomass burning events, would not be well represented in a chemical transport model using 1^o x1^o degree or 100 km^2 grid resolution. The goal of any of these isotope-enabled models should not be to assume that the existing chemistry or emissions are correct and to "tune" the isotopes in model in order for the model output to match isotope observations, rather the isotopes should be used as a constraint on whether the existing chemistry or emissions are indeed correct. In other words, mismatches between isotope enabled model predictions and the variation observed in the troposphere are indicators of gaps in our knowledge about the photochemistry that generates NO_y and could suggest how to fill those very gaps.

References

Aber J, McDowell W, Nadelhoffer K, Magill A, Berntson G, Kamakea M, McNulty S, Currie W, Rustad L, and Fernandez I (1998) Nitrogen saturation in temperate forest ecosystems - Hypotheses revisited. *Bioscience* 48(11): 921–934.

Alan DM and Andrew W (1997) *Compendium of chemical terminology: IUPAC recommendations*, 2nd edn, 1997. Malden, MA: Blackwell Science. Oxford [Oxfordshire].

Albertin S, Savarino J, Bekki S, Barbero A, and Caillon N (2021) Measurement report: Nitrogen isotopes (^{15}N) and first quantification of oxygen isotope anomalies ($\Delta^{17}O$, $\delta^{18}O$) in atmospheric nitrogen dioxide. *Atmospheric Chemistry and Physics* 21(13): 10477–10497. https://doi.org/10.5194/acp-21-10477-2021.

Alexander B, Hastings MG, Allman DJ, Dachs J, Thornton JA, and Kunasek SA (2009a) Quantifying atmospheric nitrate formation pathways based on a global model of the oxygen isotopic composition ($\Delta^{17}O$) of atmospheric nitrate. *Atmospheric Chemistry and Physics* 9(14): 5043–5056. https://doi.org/10.5194/acp-9-5043-2009.

Alexander B, Park RJ, Jacob DJ, and Gong SL (2009b) Transition metal-catalyzed oxidation of atmospheric sulfur: Global implications for the sulfur budget. *Journal of Geophysical Research-Atmospheres* 114. https://doi.org/10.1029/2008jd010486.

Alexander B, Sherwen T, Holmes CD, Fisher JA, Chen QJ, Evans MJ, and Kasibhatla P (2020) Global inorganic nitrate production mechanisms: Comparison of a global model with nitrate isotope observations. *Atmospheric Chemistry and Physics* 20(6): 3859–3877. https://doi.org/10.5194/acp-20-3859-2020.

Amundson R, Austin AT, Schuur EAG, Yoo K, Matzek V, Kendall C, Uebersax A, Brenner D, and Baisden WT (2003) Global patterns of the isotopic composition of soil and plant nitrogen. *Global Biogeochemical Cycles* 17(1).

Barkan E and Luz B (2007) Diffusivity fractionations of $H_2^{16}O/H_2^{17}O$ and $H_2^{16}O/H_2^{18}O$ in air and their implications for isotope hydrology. *Rapid Communications in Mass Spectrometry* 21(18): 2999–3005. https://doi.org/10.1002/rcm.3180.

Begun GM and Fletcher WH (1960) Partition function ratios for molecules containing nitrogen isotopes. *Journal of Chemical Physics* 33(4): 1083–1085.

Bekker C, Walters WW, Murray LT, and Hastings MG (2023) Nitrate chemistry in the northeast US – Part 1: Nitrogen isotope seasonality tracks nitrate formation chemistry. *Atmospheric Chemistry and Physics* 23(7): 4185–4201. https://doi.org/10.5194/acp-23-4185-2023.

Bender M, Sowers T, and Labeyrie L (1994) The Dole effect and its variations during the last 130,000 years as measured in the Vostok ice core. *Global Biogeochemical Cycles* 8(3): 363–376.

Bhattacharya SK, Pandey A, and Savarino J (2008) Determination of intramolecular isotope distribution of ozone by oxidation reaction with silver metal. *Journal of Geophysical Research-Atmospheres* 113: D03303. https://doi.org/10.1029/2006JD008309.

Bhetanabhotla MN, Crowell BA, Coucouvinos A, Hill RD, and Rinker RG (1985) Simulation of trace species production by lightning and corona discharge in moist air. *Atmospheric Environment* 19(9): 1391–1397. https://doi.org/10.1016/0004-6981(85)90276-8.

Bigeleisen J (1961) Statistical mechanics of isotope effects on the thermodynamic properties of condensed systems. *The Journal of Chemical Physics* 34(5): 1485–1493.

Bigeleisen J and Mayer MG (1947) Calculation of equilibrium constants for isotopic exchange reactions. *The Journal of Chemical Physics* 15(5): 261–267.

Bigeleisen J and Wolfsberg M (1958) Theoretical and experimental aspects of isotope effects in chemical kinetics. *Advances in Chemical Physics* vol. 1: 15–76 (Prigogine, I. Interscience Publishers, Inc., New York).

Blake GA, Liang MC, Morgan CG, and Yung YL (2003) A born-oppenheimer photolysis model of N_2O fractionation. *Geophysical Research Letters* 30(12): 58/51–58/54.

Blum DE, Walters WW, and Hastings MG (2020) Speciated collection of nitric acid and fine particulate nitrate for nitrogen and oxygen stable isotope determination. *Analytical Chemistry* 92(24): 16079–16088. https://doi.org/10.1021/acs.analchem.0c03696.

Blum DE, et al. (2023) Collection of nitrogen dioxide for nitrogen and oxygen isotope determination-laboratory and environmental chamber evaluation. *Analytical Chemistry*. https://doi.org/10.1021/acs.analchem.2c04672.

Bowen GJ and Revenaugh J (2003) Interpolating the isotopic composition of modern meteoric precipitation. *Water Resources Research* 39(10).

Brimblecombe P, Hara H, and Houle D (2007) *Acid Rain - Deposition to Recovery*. Springer.

Brune WH, McFarland PJ, Bruning E, Waugh S, MacGorman D, Miller DO, Jenkins JM, Ren X, Mao J, and Peischl J (2021) Extreme oxidant amounts produced by lightning in storm clouds. *Science* 372(6543): 711-+. https://doi.org/10.1126/science.abg0492.

Buda AR and DeWalle DR (2009) Using atmospheric chemistry and storm track information to explain the variation of nitrate stable isotopes in precipitation at a site in central Pennsylvania, USA. *Atmospheric Environment* 43(29): 4453–4464.

Chai JJ and Hastings MG (2018) Collection method for isotopic analysis of gaseous nitrous acid. *Analytical Chemistry* 90(1): 830–838. https://doi.org/10.1021/acs.analchem.7b03561.

Chai JJ, et al. (2019) Isotopic characterization of nitrogen oxides (NO_x), nitrous acid (HONO), and nitrate (pNO_3^-) from laboratory biomass burning during FIREX. *Atmospheric Measurement Techniques* 12(12): 6303–6317. https://doi.org/10.5194/amt-12-6303-2019.

Chameides WL, Stedman DH, Dickerson RR, Rusch DW, and Cicerone RJ (1977) NO_x production in lightning. *Journal of the Atmospheric Sciences* 34(1): 143–149. https://doi.org/10.1175/1520-0469.

Chang WL, Bhave PV, Brown SS, Riemer N, Stutz J, and Dabdub D (2011) Heterogeneous atmospheric chemistry, ambient measurements, and model calculations of N_2O_5: A review. *Aerosol Science and Technology* 45(6): 665–695.

Chang YH, Zhang YL, Tian CG, Zhang SC, Ma XY, Cao F, Liu XY, Zhang WQ, Kuhn T, and Lehmann MF (2018) Nitrogen isotope fractionation during gas-to-particle conversion of NO_x to NO_3^- in the atmosphere - implications for isotope-based NO_x source apportionment. *Atmospheric Chemistry and Physics* 18(16): 11647–11661. https://doi.org/10.5194/acp-18-11647-2018.

Chapman PJ and Edwards AC (1999) The impact of atmospheric nitrogen deposition on the behavior of nitrogen in surface waters. In: Langan SJ (ed.) *Impact of Nitrogen Deposition on Natural and Semi-Natural Ecosystems*, pp. 153–212. Boston: Kluwer Academic.

Chen D, Rojas M, Samset BH, Cobb K, Niang AD, Edwards P, Emori S, Faria SH, Hawkins E, Hope P, Huybrechts P, Meinshausen M, Mustafa SK, Plattner G-K, and Tréguier A-M (2021) In climate change 2021: The physical science basis. In: *Contribution of Working Group I to the Sixth Assessment Report of the Intergovernmental Panel on Climate Change*, pp. 147–286. Cambridge, United Kingdom and New York, NY, USA: Cambridge University Press. https://doi.org/10.1017/9781009157896.003. Cambridge, United Kingdom and New York, NY, USA.

Coplen TB and Shrestha Y (2016) Isotope-abundance variations and atomic weights of selected elements: 2016 (IUPAC Technical Report). *Pure and Applied Chemistry* 88(12): 1203–1224. https://doi.org/10.1515/pac-2016-0302.

Craine JM, Brookshire ENJ, Cramer MD, Hasselquist NJ, Koba K, Marin-Spiotta E, and Wang LX (2015) Ecological interpretations of nitrogen isotope ratios of terrestrial plants and soils. *Plant and Soil* 396(1-2): 1–26. https://doi.org/10.1007/s11104-015-2542-1.

Criss RE (1999) *Principles of Stable Isotope Distribution*. New York: Oxford University Press.

Dahal B and Hastings MG (2016) Technical considerations for the use of passive samplers to quantify the isotopic composition of NOx and NO_2 using the denitrifier method. *Atmospheric Environment* 143: 60–66. https://doi.org/10.1016/j.atmosenv.2016.08.006.

Dentener FJ and Crutzen PJ (1993) Reaction of N_2O_5 on tropospheric aerosols: Impact on the global distributions of NO_x, O_3, and OH. *Journal of Geophysical Research – Atmospheres* 98(D4): 7149–7163. https://doi.org/10.1029/92JD02979.

Dole M, Lane GA, Rudd DP, and Zaukelies DA (1954) Isotopic composition of atmospheric oxygen and nitrogen. *Geochimica et Cosmochimica Acta* 6(2-3): 65–78.

Elliott EM, Kendall C, Wankel SD, Burns DA, Boyer EW, Harlin K, Bain DJ, and Butler TJ (2007) Nitrogen isotopes as indicators of NO_x source contributions to atmospheric nitrate deposition across the Midwestern and northeastern United States. *Environmental Science & Technology* 41(22): 7661–7667.

Elliott EM, Yu ZJ, Cole AS, and Coughlin JG (2019) Isotopic advances in understanding reactive nitrogen deposition and atmospheric processing. *Science of the Total Environment* 662: 393–403. https://doi.org/10.1016/j.scitotenv.2018.12.177.

Fan MY, Zhang WQ, Zhang YL, Li JHY, Fang H, Cao F, Yan M, Hong YH, Guo H, and Michalski G (2023) Formation mechanisms and source apportionments of nitrate aerosols in a megacity of Eastern China based on multiple isotope observations. *Journal of Geophysical Research-Atmospheres* 128(6). https://doi.org/10.1029/2022jd038129.

Fang H and Michalski G (2022) Assessing the roles emission sources and atmospheric processes play in simulating $\delta^{15}N$ of atmospheric NO_x and NO_3^- using CMAQ (version 5.2.1) and SMOKE (version 4.6). *Geoscientific Model Development* 15(10): 4239–4258. https://doi.org/10.5194/gmd-15-4239-2022.

Fang H, Walters WW, Mase D, and Michalski G (2021) $_N$RACM: Incorporating ^{15}N into the regional atmospheric chemistry mechanism (RACM) for assessing the role photochemistry plays in controlling the isotopic composition of NO_x, NO_y, and atmospheric nitrate. *Geoscientific Model Development* 14(8): 5001–5022. https://doi.org/10.5194/gmd-14-5001-2021.

Felix JD and Elliott EM (2014) Isotopic composition of passively collected nitrogen dioxide emissions: Vehicle, soil and livestock source signatures. *Atmospheric Environment* 92: 359–366. https://doi.org/10.1016/j.atmosenv.2014.04.005.

Felix JD, Elliott EM, and Shaw SL (2012) Nitrogen isotopic composition of coal-fired power plant NO_x: Influence of emission controls and implications for global emission inventories. *Environmental Science & Technology* 46(6): 3528–3535.

Fenn ME, Baron JS, Allen EB, Rueth HM, Nydick KR, Geiser L, Bowman WD, Sickman JO, Meixner T, Johnson DW, and Neitlich P (2003) Ecological effects of nitrogen deposition in the western United States. *Bioscience* 53(4): 404–420.

Fibiger DL and Hastings MG (2016) First measurements of the nitrogen isotopic composition of NOx from biomass burning. *Environmental Science & Technology* 50(21): 11569–11574. https://doi.org/10.1021/acs.est.6b03510.

Finlayson-Pitts BJ and Pitts JN Jr (2000) *Chemistry of the Upper and Lower Atmosphere*. San Diego: Academic Press.

Freyer HD (1978) Seasonal trends of NH_4^+ and NO_3^- nitrogen isotope composition in rain collected at Julich, Germany. *Tellus* 30(1): 83–92.

Freyer HD (1991) Seasonal-variation of $^{15}N/^{14}N$ ratios in atmospheric nitrate species. *Tellus Series B: Chemical and Physical Meteorology* 43(1): 30–44.

Freyer HD, Kley D, Volzthomas A, and Kobel K (1993) On the interaction of isotopic exchange processes with photochemical-reactions in atmospheric oxides of nitrogen. *Journal of Geophysical Research-Atmospheres* 98(D8): 14791–14796. https://doi.org/10.1029/93jd00874.

Friedman L and Bigeleisen J (1950) Oxygen and nitrogen isotope effects in the decomposition of ammonium nitrate. *The Journal of Chemical Physics* 18(10): 1325–1331.

Gao YQ and Marcus RA (2001) Strange and unconventional isotope effects in ozone formation. *Science* 293(5528): 259–263.

Gat JR (1996) Oxygen and hydrogen isotopes in the hydrologic cycle. *Annual Review of Earth and Planetary Sciences* 24: 225–262. https://doi.org/10.1146/annurev.earth.24.1.225.

Goldenbaum GC and Dickerson RR (1993) Nitric-oxide production by lightning discharges. *Journal of Geophysical Research-Atmospheres* 98(D10): 18333–18338. https://doi.org/10.1029/93jd01018.

Greenblatt GD and Howard CJ (1989) Oxygen atom exchange in the interaction of hydroxyl-(^{18}OH) with several small molecules. *Journal of Physical Chemistry* 93(3): 1035–1042.

Griffis TJ, Wood JD, Baker JM, Lee X, Xiao K, Chen Z, Welp LR, Schultz NM, Gorski G, Chen M, and Nieber J (2016) Investigating the source, transport, and isotope composition of water vapor in the planetary boundary layer. *Atmospheric Chemistry and Physics* 16(8): 5139–5157. https://doi.org/10.5194/acp-16-5139-2016.

Guha T, Lin CT, Bhattacharya SK, Mahajan AS, Ou-Yang CF, Lan YP, Hsu SC, and Liang MC (2017) Isotopic ratios of nitrate in aerosol samples from Mt. Lulin, a high-altitude station in Central Taiwan. *Atmospheric Environment* 154: 53–69. https://doi.org/10.1016/j.atmosenv.2017.01.036.

Hastings MG, Sigman DM, and Lipschultz F (2003) Isotopic evidence for source changes of nitrate in rain at Bermuda. *Journal of Geophysical Research-Atmospheres* 108(D24).

Heaton THE (1987) ^{15}N/^{14}N ratios of nitrate and ammonium in rain at Pretoria, South Africa. *Atmospheric Environment* 21(4): 843–852.

Heidenreich JE III and Thiemens MH (1983) A non-mass-dependent isotope effect in the production of ozone from molecular oxygen. *Journal of Chemical Physics* 78(2): 892–895.

Hill RD (1979) Production of nitric-oxide by lightning. *Geophysical Research Letters* 6(12): 945–947. https://doi.org/10.1029/GL006i012p00945.

Hoering T (1957) The isotopic composition of the ammonia and the nitrate ion in rain. *Geochimica et Cosmochimica Acta* 12(1-2): 97–102.

Hogberg P (1997) Tansley review No 95 - ^{15}N natural abundance in soil-plant systems. *New Phytologist* 137(2): 179–203.

Holt BD, Kumar R, and Cunningham PT (1982) Primary sulfates in atmospheric sulfates - estimation by oxygen isotope ratio measurements. *Science* 217(4554): 51–53.

Homyak PM, Blankinship JC, Marchus K, Lucero DM, Sickman JO, and Schimel JP (2016) Aridity and plant uptake interact to make dryland soils hotspots for nitric oxide (NO) emissions. *Proceedings of the National Academy of Sciences of the United States of America* 113(19): E2608–E2616. https://doi.org/10.1073/pnas.1520496113.

Huang SN, Wang F, Elliott EM, Zhu FF, Zhu WX, Koba K, Yu ZJ, Hobbie EA, Michalski G, Kang RH, Wang AZ, Zhu JJ, Fu SL, and Fang YT (2020) Multiyear measurements on Δ^{17}O of stream nitrate indicate high nitrate production in a temperate forest. *Environmental Science & Technology* 54(7): 4231–4239. https://doi.org/10.1021/acs.est.9b07839.

Huang SN, Fang YT, Zhu FF, Elliott EM, Felix JD, Wang F, Li SL, Liu DW, Song LL, Li ZJ, Fu PQ, and Fu SL (2021) Multiyear measurements on ^{15}N natural abundance of precipitation nitrate at a rural forested site. *Atmospheric Environment* 253. https://doi.org/10.1016/j.atmosenv.2021.118353.

Ingerson E (1953) Nonradiogenic isotopes in geology - A review. *Geological Society of America Bulletin* 64(3): 301–373. https://doi.org/10.1130/0016-7606.

Janssen C, Guenther J, Krankowsky D, and Mauersberger K (1999) Relative formation rates of $^{50}O_3$ and $^{52}O_3$ in ^{16}O,^{18}O mixtures. *Journal of Chemical Physics* 111(16): 7179–7182.

Janssen C, Guenther J, Mauersberger K, and Krankowsky D (2001) Kinetic origin of the ozone isotope effect: A critical analysis of enrichments and rate coefficients. *Physical Chemistry Chemical Physics* 3(21): 4718–4721.

Janssen C, Guenther J, Krankowsky D, and Mauersberger K (2003) Temperature dependence of ozone rate coefficients and isotopologue fractionation in ^{16}O,^{18}O mixtures oxygen mixtures. *Chemical Physics Letters* 367(1-2): 34–38.

Johnston JC and Thiemens MH (1997) The isotopic composition of tropospheric ozone in three environments. *Journal of Geophysical Research* 102(D21): 25395–25404.

Kaiser J, Hastings MG, Houlton BZ, Rockmann T, and Sigman DM (2007) Triple oxygen isotope analysis of nitrate using the denitrifier method and thermal decomposition of N_2O. *Analytical Chemistry* 79: 599–607.

Kawashima H (2019) Seasonal trends of the stable nitrogen isotope ratio in particulate nitrogen compounds and their gaseous precursors in Akita, Japan. *Tellus Series B: Chemical and Physical Meteorology* 71. https://doi.org/10.1080/16000889.2019.1627846.

Kaye JA (1992) Isotope effects in gas-phase chemical reactions and photodissociation processes. Overview. In: *American Chemical Society Symposium Series, 502 (Isot. Eff. Gas-Phase Chem.),* pp. 1–14.

Kendall C (1998) Tracing nitrogen sources and cycling in catchments. In: Kendall C and McDonnell JJ (eds.) *Isotope Tracers in Catchment Hydrology,* pp. 519–576. Amsterdam: Elsevier Science.

Kim H, Walters WW, Bekker C, Murray LT, and Hastings MG (2023) Nitrate chemistry in the northeast US - Part 2: Oxygen isotopes reveal differences in particulate and gas-phase formation. *Atmospheric Chemistry and Physics* 23(7): 4203–4219. https://doi.org/10.5194/acp-23-4203-2023.

Krankowsky D, Bartecki F, Klees GG, Mauersberger K, Schellenbach K, and Stehr J (1995) Measurement of heavy isotope enrichment in tropospheric ozone. *Geophysical Research Letters* 22(13): 1713–1716.

Kroopnick P and Craig H (1972) Atmospheric oxygen. Isotopic composition and solubility fractionation. *Science* 175(4017): 54–55.

Leibensperger EM, Mickley LJ, Jacob DJ, Chen WT, Seinfeld JH, Nenes A, Adams PJ, Streets DG, Kumar N, and Rind D (2012) Climatic effects of 1950-2050 changes in US anthropogenic aerosols - Part 1: Aerosol trends and radiative forcing. *Atmospheric Chemistry and Physics* 12(7): 3333–3348.

Lelieveld J, Evans JS, Fnais M, Giannadaki D, and Pozzer A (2015) The contribution of outdoor air pollution sources to premature mortality on a global scale. *Nature* 525(7569). https://doi.org/10.1038/nature15371.

Li DJ and Wang XM (2008) Nitrogen isotopic signature of soil-released nitric oxide (NO) after fertilizer application. *Atmospheric Environment* 42(19): 4747–4754.

Li J, Zhang X, Orlando J, Tyndall G, and Michalski G (2020) Quantifying the nitrogen isotope effects during photochemical equilibrium between NO and NO_2: Implications for δ^{15}N in tropospheric reactive nitrogen. *Atmospheric Chemistry and Physics* 20(16): 9805–9819. https://doi.org/10.5194/acp-20-9805-2020.

Liang MC, Blake GA, and Yung YL (2004) A semianalytic model for photo-induced isotopic fractionation in simple molecules. *Journal of Geophysical Research-Atmospheres* 109(D10).

Lighty JS, Veranth JM, and Sarofim AF (2000) Combustion aerosols: Factors governing their size and composition and implications to human health. *Journal of the Air & Waste Management Association* 50(9): 1565–1618. https://doi.org/10.1080/10473289.2000.10464197.

Liu J, Li S, Mekic M, Jiang H, Zhou W, Loisel G, Song W, Wang X, and Gligorovski S (2019) Photoenhanced uptake of NO_2 and HONO formation on real urban grime. *Environmental Science & Technology Letters* 6. https://doi.org/10.1021/acs.estlett.9b00308.

Liu XY, Yin YM, and Song W (2020) Nitrogen isotope differences between major atmospheric NO_y species: Implications for transformation and deposition processes. *Environmental Science & Technology Letters* 7(4): 227–233. https://doi.org/10.1021/acs.estlett.0c00105.

Luz B and Barkan E (2000) Assessment of oceanic productivity with the triple-isotope composition of dissolved oxygen. *Science* 288(5473): 2028–2031.

Luz B and Barkan E (2005) The isotopic ratios ^{17}O/^{16}O and ^{18}O/^{16}O in molecular oxygen and their significance in biogeochemistry. *Geochimica et Cosmochimica Acta* 69(5): 1099–1110.

Luz B, Barkan E, Bender ML, Thiemens MH, and Boering KA (1999) Triple-isotope composition of atmospheric oxygen as a tracer of biosphere productivity. *Nature* 400(6744): 547–550.

Luz B, Barkan E, Yam R, and Shemesh A (2009) Fractionation of oxygen and hydrogen isotopes in evaporating water. *Geochimica et Cosmochimica Acta* 73(22): 6697–6703. https://doi.org/10.1016/j.gca.2009.08.008.

Lynch JA, Bowersox VC, and Grimm JW (2000) Acid rain reduced in eastern United States. *Environmental Science & Technology* 34(6): 940–949.

Lyons JR (2001) Transfer of mass-independent fractionation in ozone to other oxygen-containing radicals in the atmosphere. *Geophysical Research Letters* 28(17): 3231–3234.

Marcus RA (2004) *Chemical Dynamics at the Turn of the Century: Nobel Laureates Look Back and Ahead.* American Chemical Society Annual Meeting.

Masterson AL, Farquhar J, and Wing BA (2011) Sulfur mass-independent fractionation patterns in the broadband UV photolysis of sulfur dioxide: Pressure and third body effects. *Earth and Planetary Science Letters* 306(3-4): 253–260. https://doi.org/10.1016/j.epsl.2011.04.004.

Mauersberger K, Morton J, Schueler B, Stehr J, and Anderson SM (1993) Multi-isotope study of ozone - Implications for the heavy ozone anomaly. *Geophysical Research Letters* 20(11): 1031–1034.

Mauersberger K, Krankowsky D, and Janssen C (2003) Oxygen isotope processes and transfer reactions. *Space Science Reviews* 106(1-4): 265–279.

Meijer HAJ and Li WJ (1998) The use of electrolysis for accurate δ^{17}O and δ^{18}O isotope measurements in water. *Isotopes in Environmental and Health Studies* 34(4): 349–369.

Michalski G and Bhattacharya SK (2009) The role of symmetry in the mass independent isotope effect in ozone. *Proceedings of the National Academy of Sciences* 106(280): 11496–11501.

Michalski G, Scott Z, Kabiling M, and Thiemens M (2003) First measurements and modeling of Δ^{17}O in atmospheric nitrate. *Geophysical Research Letters 30*(16). 1870.

Michalski G, Meixner T, Fenn M, Hernandez L, Sirulnik A, Allen E, and Thiemens M (2004) Tracing atmospheric nitrate deposition in a complex semiarid ecosystem using Δ^{17}O. *Environmental Science & Technology* 38(7): 2175–2181.

Michalski G, Bhattacharya SK, and Mase D (2011) Oxygen Isotope Dynamics of Atmospheric Nitrate and Its Precursor Molecules. In: Baskaran M (ed.) *The Handbook of Environmental Isotope Geochemistry*, pp. 613–638. Springer.

Michalski G, Bhattacharya S, and Girsch G (2014) NO_x cycle and the tropospheric ozone isotope anomaly: An experimental investigation. *Atmospheric Chemistry and Physics* 14(10): 4935–4953.

Michalski G, Kolanowski M, and Riha KM (2015) Oxygen and nitrogen isotopic composition of nitrate in commercial fertilizers, nitric acid, and reagent salts. *Isotopes in Environmental and Health Studies* 51(3): 382–391. https://doi.org/10.1080/10256016.2015.1054821.

Michalski G, Larrea Valdivia AE, Olson E, Welp L, Fang H, Magara-Gomez K, Morales Paredes L, Reyes Larico J, and Li J (2022) Identifying NO_x sources in arequipa, peru using nitrogen isotopes in particulate nitrate. *Frontiers in Environmental Science* 10. https://doi.org/10.3389/fenvs.2022.916738.

Miller MF (2002) Isotopic fractionation and the quantification of ^{17}O anomalies in the oxygen three-isotope system: An appraisal and geochemical significance. *Geochimica et Cosmochimica Acta* 66(11): 1881–1889.

Miller CE and Yung YL (2000) Photo-induced isotopic fractionation. *Journal of Geophysical Research-Atmospheres* 105(D23): 29039–29051.

Miller DJ, Wojtal PK, Clark SC, and Hastings MG (2017) Vehicle NO_x emission plume isotopic signatures: Spatial variability across the eastern United States. *Journal of Geophysical Research-Atmospheres* 122(8): 4698–4717. https://doi.org/10.1002/2016jd025877.

Miller DJ, Chai JJ, Guo F, Dell CJ, Karsten H, and Hastings MG (2018) Isotopic composition of in situ soil NO_x emissions in manure-fertilizes cropland. *Geophysical Research Letters* 45(21): 12058–12066. https://doi.org/10.1029/2018gl079619.

Monks PS (2005) Gas-phase radical chemistry in the troposphere. *Chemical Society Reviews* 34(5): 376–395. https://doi.org/10.1039/b307982c.

Morin S, Savarino J, Frey MM, Yan N, Bekki S, Bottenheim JW, and Martins JMF (2008) Tracing the origin and fate of NO_x in the Arctic atmosphere using stable isotopes in nitrate. *Science* 322(5902): 730–732.

Morin S, Savarino J, Frey MM, Domine F, Jacobi HW, Kaleschke L, and Martins JMF (2009) Comprehensive isotopic composition of atmospheric nitrate in the Atlantic Ocean boundary layer from 65º S to 79º N. *Journal of Geophysical Research-Atmospheres* 114: D05303. https://doi.org/10.1029/2008JD010696.

Morin S, Sander R, and Savarino J (2011) Simulation of the diurnal variations of the oxygen isotope anomaly ($\Delta^{17}O$) of reactive atmospheric species. *Atmospheric Chemistry and Physics* 11(8): 3653–3671. https://doi.org/10.5194/acp-11-3653-2011.

Morino Y, Kondo Y, Takegawa N, Miyazaki Y, Kita K, Komazaki Y, Fukuda M, Miyakawa T, Moteki N, and Worsnop DR (2006) Partitioning of HNO_3 and particulate nitrate over Tokyo: Effect of vertical mixing. *Journal of Geophysical Research-Atmospheres* 111(D15). https://doi.org/10.1029/2005jd006887.

Nelson DM, Tsunogai U, Ding D, Ohyama T, Komatsu DD, Nakagawa F, Noguchi I, and Yamaguchi T (2018) Triple oxygen isotopes indicate urbanization affects sources of nitrate in wet and dry atmospheric deposition. *Atmospheric Chemistry and Physics* 18(9): 6381–6392. https://doi.org/10.5194/acp-18-6381-2018.

Orville RE (1968) A cooperative experiment on lightning discharge. *Bulletin of the American Meteorological Society* 49(10): 1030.

Paerl HW, Boynton WR, Dennis RL, Driscoll CT, Greening HS, Kremer JN, Rabalais N, and Seitzinger SP (2001) Atmospheric deposition of nitrogen in coastal waters: Biogeochemical and ecological implications. In: Valigura RA, Alexander RB, Castro MS, Meyers T, Paerl HW, Stacey PE, and Turner RE (eds.) *Nitrogen Loading in Coastal Water Bodies: An Atmospheric Perspective*, pp. 11–52. Washington: American Geophysical Union.

Paerl HW, Dennis RL, and Whitall DR (2002) Atmospheric deposition of nitrogen: Implications for nutrient over-enrichment of coastal waters. *Estuaries* 25(4B): 677–693.

Pan YP, Gu MN, He YX, Wu DM, Liu CY, Song LL, Tian SL, Lu XM, Sun Y, Song T, Walters WW, Liu XJ, Martin NA, Zhang QQ, Fang YT, Ferracci V, and Wang YS (2020) Revisiting the concentration observations and source apportionment of atmospheric ammonia. *Advances in Atmospheric Sciences* 37(9): 933–938. https://doi.org/10.1007/s00376-020-2111-2.

Parnell AC, Phillips DL, Bearhop S, Semmens BX, Ward EJ, Moore JW, Jackson AL, Grey J, Kelly DJ, and Inger R (2013) Bayesian stable isotope mixing models. *Environmetrics* 10(1-2): 387–399. https://doi.org/10.1002/env.2221.

Paulot F, Ginoux P, Cooke WF, Donner LJ, Fan S, Lin MY, Mao J, Naik V, and Horowitz LW (2016) Sensitivity of nitrate aerosols to ammonia emissions and to nitrate chemistry: Implications for present and future nitrate optical depth. *Atmospheric Chemistry and Physics* 16(3): 1459–1477. https://doi.org/10.5194/acp-16-1459-2016.

Pollack IB, Homeyer CR, Ryerson TB, Aikin KC, Peischl J, Apel EC, Campos T, Flocke F, Hornbrook RS, Knapp DJ, Montzka DD, Weinheimer AJ, Riemer D, Diskin G, Sachse G, Mikoviny T, Wisthaler A, Bruning E, MacGorman D, Cummings KA, Pickering KE, Huntrieser H, Lichtenstern M, Schlager H, and Barth MC (2016) Airborne quantification of upper tropospheric NO_x production from lightning in deep convective storms over the United States Great Plains. *Journal of Geophysical Research-Atmospheres* 121(4): 2002–2028. https://doi.org/10.1002/2015jd023941.

Proemse BC, Mayer B, Chow JC, and Watson JG (2012) Isotopic characterization of nitrate, ammonium and sulfate in stack $PM_{2.5}$ emissions in the Athabasca Oil Sands Region, Alberta, Canada. *Atmospheric Environment* 60: 555–563. https://doi.org/10.1016/j.atmosenv.2012.06.046.

Rahn T, Zhang H, Wahlen M, and Blake GA (1998) Stable isotope fractionation during ultraviolet photolysis of N_2O. *Geophysical Research Letters* 25(24): 4489–4492.

Rayleigh L (1902) On the distillation of binary mixtures. *Philosophical Magazine* 4: 521–537.

Redling K, Elliott E, Bain D, and Sherwell J (2013) Highway contributions to reactive nitrogen deposition: Tracing the fate of vehicular NOx using stable isotopes and plant biomonitors. *Biogeochemistry* 116(1-3): 261–274.

Richet P, Bottinga Y, and Javoy M (1977) Review of hydrogen, carbon, nitrogen, oxygen, sulfur, and chlorine stable isotope fractionation among gaseous molecules. *Annual Review of Earth and Planetary Sciences* 5: 65–110.

Riha KM (2014) *The Use of Stable Isotopes to Constrain the Nitrogen Cycle*. Dissertation thesis,. West Lafayette, IN: Purdue University.

Riha KM, Michalski G, Gallo EL, Lohse KA, Brooks PD, and Meixner T (2014) High atmospheric nitrate inputs and nitrogen turnover in semi-arid urban catchments. *Ecosystems* 17(8): 1309–1325.

Rose LA, Yu ZJ, Bain DJ, and Elliott EM (2019) High resolution, extreme isotopic variability of precipitation nitrate. *Atmospheric Environment* 207: 63–74. https://doi.org/10.1016/j.atmosenv.2019.03.012.

Savarino J and Thiemens MH (1999a) Analytical procedure to determine both $\delta^{18}O$ and $\delta^{17}O$ of H_2O_2 in natural water and first measurements. *Atmospheric Environment* 33(22): 3683–3690.

Savarino J and Thiemens MH (1999b) Mass-independent oxygen isotope (^{16}O, ^{17}O, ^{18}O) fractionation found in Hx,Ox reactions. *Journal of Physical Chemistry A* 103(46): 9221–9229.

Savarino J, Lee CCW, and Thiemens MH (2000) Laboratory oxygen isotopic study of sulfur (IV) oxidation: Origin of the mass-independent oxygen isotopic anomaly in atmospheric sulfates and sulfate mineral deposits on Earth. *Journal of Geophysical Research* 105(D23): 29079–29088.

Savarino J, Kaiser J, Morin S, Sigman DM, and Thiemens MH (2007) Nitrogen and oxygen isotopic constraints on the origin of atmospheric nitrate in coastal Antarctica. *Atmospheric Chemistry and Physics* 7(8): 1925–1945. https://doi.org/10.5194/acp-7-1925-2007.

Schwartz J and Neas LM (2000) Fine particles are more strongly associated than coarse particles with acute respiratory health effects in schoolchildren. *Epidemiology* 11(1): 6–10.

Shi YS, Tian P, Jin ZF, Hu YM, Zhang YQ, and Li FL (2022) Stable nitrogen isotope composition of NO_x of biomass burning in China. *Science of the Total Environment* 803. https://doi.org/10.1016/j.scitotenv.2021.149857.

Sofen ED, Alexander B, and Kunasek SA (2011) The impact of anthropogenic emissions on atmospheric sulfate production pathways, oxidants, and ice core $\Delta^{17}O$ (SO_4^{2-}). *Atmospheric Chemistry and Physics* 11(7): 3565–3578. https://doi.org/10.5194/acp-11-3565-2011.

Song W, Liu XY, Hu CC, Chen GY, Liu XJ, Walters WW, Michalski G, and Liu CQ (2021) Important contributions of non-fossil fuel nitrogen oxides emissions. *Nature Communications* 12(1): 243. https://doi.org/10.1038/s41467-020-20356-0.

Stein AF, Draxler RR, Rolph GD, Stunder BJB, Cohen MD, and Ngan F (2015) NOAA's HYSPLIT atmospheric transport and dispersion modeling system. *Bulletin of the American Meteorological Society* 96(12): 2059–2077. https://doi.org/10.1175/BAMS-D-14-00110.1.

Stockwell WR, Kirchner F, Kuhn M, and Seefeld S (1997) A new mechanism for regional atmospheric chemistry modeling. *Journal of Geophysical Research* 102(D22): 25847–25879. https://doi.org/10.1029/97JD00849.

Su CX, Kang RH, Zhu WX, Huang WT, Song LL, Wang A, Liu DW, Quan Z, Zhu FF, Fu PQ, and Fang YT (2020) $\delta^{15}N$ of nitric oxide produced under aerobic or anaerobic conditions from seven soils and their associated N isotope fractionations. *Journal of Geophysical Research – Biogeosciences* 125(9). https://doi.org/10.1029/2020jg005705.

Sun Z, Zong Z, Tan Y, Tian C, Liu Z, Zhang F, Sun R, Chen Y, Li J, and Zhang G (2023) Characterization of the nitrogen stable isotope composition ($\delta^{15}N$) of ship-emitted NO_x. *Atmospheric Chemistry and Physics* 23(19): 12851–12865. https://doi.org/10.5194/acp-23-12851-2023.

Thiemens MH (2005) A survey of mass independent isotope effects in nature. *Geochimica et Cosmochimica Acta* 69(10): A443.

Thiemens MH (2013) Introduction to chemistry and applications in nature of mass independent isotope effects special feature. *Proceedings of the National Academy of Sciences of the United States of America* 110(44): 17631–17637. https://doi.org/10.1073/pnas.1312926110.

Thiemens MH and Heidenreich JE III (1983) The mass-independent fractionation of oxygen: A novel isotope effect and its possible cosmochemical implications. *Science* 219(4588): 1073–1075.

Thiemens MH, Savarino J, Farquhar J, and Bao H (2001) Mass-independent isotopic compositions in terrestrial and extraterrestrial solids and their applications. *Accounts of Chemical Research* 34(8): 645–652.

Tian J, Guan H, Zhou YH, Zheng NJ, Xiao HW, Zhao JJ, Zhang ZY, and Xiao HY (2021) Isotopic source analysis of nitrogen-containing aerosol: A study of $PM_{2.5}$ in Guiyang (SW, China). *Science of the Total Environment* 760. https://doi.org/10.1016/j.scitotenv.2020.143935.

Tilman D, Wedin D, and Knops J (1996) Productivity and sustainability influenced by biodiversity in grassland ecosystems. *Nature* 379(6567): 718–720.

Uemura R, Barkan E, Abe O, and Luz B (2010) Triple isotope composition of oxygen in atmospheric water vapor. *Geophysical Research Letters* 37.

Urey HC (1947) Thermodynamic properties of isotopic substances. *Journal of the Chemical Society*: 562–581.

Urey HC and Greiff LJ (1935) Isotopic exchange equilibria. *Journal of the American Chemical Society* 57(1): 321–327. https://doi.org/10.1021/ja01305a026.

Van Hook WA, Rebelo LPN, and Wolfsberg M (2001) An interpretation of the vapor phase second virial coefficient isotope effect: Correlation of virial coefficient and vapor pressure isotope effects. *Journal of Physical Chemistry A* 105(40): 9284–9297. https://doi.org/10.1021/jp004305z.

Vicars WC and Savarino J (2014) Quantitative constraints on the ^{17}O excess ($\Delta^{17}O$) signature of surface ozone: Ambient measurements from 50° N to 50° S using the nitrite-coated filter technique. *Geochimica et Cosmochimica Acta* 135: 270–287. https://doi.org/10.1016/j.gca.2014.03.023.

Vicars WC, Bhattacharya SK, Erbland J, and Savarino J (2012) Measurement of the ^{17}O excess ($\Delta^{17}O$) of tropospheric ozone using a nitrite-coated filter. *Rapid Communications in Mass Spectrometry* 26(10): 1219–1231.

Walters WW and Michalski G (2015) Theoretical calculation of nitrogen isotope equilibrium exchange fractionation factors for various NO_y molecules. *Geochimica et Cosmochimica Acta* 164: 284–297. https://doi.org/10.1016/j.gca.2015.05.029.

Walters WW and Michalski G (2016a) Ab initio study of nitrogen and position-specific oxygen kinetic isotope effects in the NO + O_3 reaction. *Journal of Chemical Physics* 145(22). https://doi.org/10.1063/1.4968562.

Walters WW and Michalski G (2016b) Theoretical calculation of oxygen equilibrium isotope fractionation factors involving various NO_y molecules, OH, and H_2O and its implications for isotope variations in atmospheric nitrate. *Geochimica et Cosmochimica Acta* 191: 89–101. https://doi.org/10.1016/j.gca.2016.06.039.

Walters WW, Goodwin S, and Michalski G (2015a) Nitrogen stable isotope composition of vehile emitted NO_x. *Environemental Science and Technology* 49(4): 2278–2285.

Walters WW, Goodwin SR, and Michalski G (2015b) Nitrogen stable isotope composition ($\delta^{15}N$) of vehicle-emitted NO_x. *Environmental Science & Technology* 49(4): 2278–2285. https://doi.org/10.1021/es505580v.

Walters WW, Tharp BD, Fang H, Kozak BJ, and Michalski G (2015c) Nitrogen isotope composition of thermally produced NOx from various fossil-fuel combustion sources. *Environmental Science & Technology* 49(19): 11363–11371. https://doi.org/10.1021/acs.est.5b02769.

Walters WW, Simonini DS, and Michalski G (2016) Nitrogen isotope exchange between NO and NO_2 and its implications for ^{15}N variations in tropospheric NO_x and atmospheric nitrate. *Geophysical Research Letters* 43(1): 440–448. https://doi.org/10.1002/2015gl066438.

Walters WW, Fang H, and Michalski G (2018) Summertime diurnal variations in the isotopic composition of atmospheric nitrogen dioxide at a small midwestern United States city. *Atmospheric Environment* 179: 1–11. https://doi.org/10.1016/j.atmosenv.2018.01.047.

Walters WW, Michalski G, Bohlke JK, Alexander B, Savarino J, and Thiemens MH (2019) Assessing the seasonal dynamics of nitrate and sulfate aerosols at the south pole utilizing stable isotopes. *Journal of Geophysical Research-Atmospheres* 124(14): 8161–8177. https://doi.org/10.1029/2019jd030517.

Wang YL, Liu XY, Song W, Yang W, Han B, Dou XY, Zhao XD, Song ZL, Liu CQ, and Bai ZP (2017) Source appointment of nitrogen in $PM_{2.5}$ based on bulk $\delta^{15}N$ signatures and a Bayesian isotope mixing model. *Tellus Series B: Chemical and Physical Meteorology* 69. https://doi.org/10.1080/16000889.2017.1299672.

Wang YL, Song W, Yang W, Sun XC, Tong YD, Wang XM, Liu CQ, Bai ZP, and Liu XY (2019) Influences of atmospheric pollution on the contributions of major oxidation pathways to $PM_{2.5}$ nitrate formation in Beijing. *Journal of Geophysical Research-Atmospheres* 124(7): 4174–4185. https://doi.org/10.1029/2019jd030284.

Wang YJ, Liu JW, Jiang F, Chen ZX, Wu LL, Zhou SZ, Pei CL, Kuang Y, Cao F, Zhang YL, Fan MY, Zheng JY, Li J, and Zhang G (2023) Vertical measurements of stable nitrogen and oxygen isotope composition of fine particulate nitrate aerosol in Guangzhou city: Source apportionment and oxidation pathway. *Science of the Total Environment* 865. https://doi.org/10.1016/j.scitotenv.2022.161239.

Wolfsberg M, Van Hook WA, Paneth P, Rebelo LPN, Wolfsberg M, VanHook WA, and Paneth P (2010) *Isotope Effects on Equilibrium Constants of Chemical Reactions; Transition State Theory of Isotope Effects*, pp. 77–137. https://doi.org/10.1007/978-90-481-2265-3_4.

Xiao HY and Liu CQ (2011) The elemental and isotopic composition of sulfur and nitrogen in Chinese coals. *Organic Geochemistry* 42(1): 84–93. https://doi.org/10.1016/j.orggeochem.2010.10.011.

Xiao HW, Wu JF, Luo L, Liu C, Xie YJ, and Xiao HY (2020) Enhanced biomass burning as a source of aerosol ammonium over cities in central China in autumn. *Environmental Pollution* 266. https://doi.org/10.1016/j.envpol.2020.115278.

Xu H, Tsunogai U, Nakagawa F, Li YJ, Ito M, Sato K, and Tanimoto H (2021) Determination of the triple oxygen isotopic composition of tropospheric ozone in terminal positions using a multistep nitrite-coated filter-pack system. *Rapid Communications in Mass Spectrometry* 35(15). https://doi.org/10.1002/rcm.9124.

Yin MJ, Guan H, Luo L, Xiao HY, and Zhang ZY (2022) Using nitrogen and oxygen stable isotopes to analyze the major NO_x sources to nitrate of PM2.5 in Lanzhou, northwest China, in winter-spring periods. *Atmospheric Environment* 276. https://doi.org/10.1016/j.atmosenv.2022.119036.

Young ED, Galy A, and Nagahara H (2002) Kinetic and equilibrium mass-dependent isotope fractionation laws in nature and their geochemical and cosmochemical significance. *Geochimica et Cosmochimica Acta* 66(6): 1095–1104.

Yu ZJ and Elliott EM (2017) Novel method for nitrogen isotopic analysis of soil-emitted nitric oxide. *Environmental Science & Technology* 51(11): 6268–6278. https://doi.org/10.1021/acs.est.7b00592.

Yung YL and Miller CE (1997) Isotopic fractionation of stratospheric nitrous oxide. *Science* 278(5344): 1778–1780.

Yvon SA, Saltzman ES, Cooper DJ, Bates TS, and Thompson AM (1996) Atmospheric sulfur cycling in the tropical Pacific marine boundary layer (12°S, 135°W): A comparison of field data and model results. 1. Dimethyl sulfide. *Journal of Geophysical Research* 101(D3): 6899–6909.

Zhang YL, Zhang W, Fan MY, Li J, Fang H, Cao F, Lin YC, Wilkins BP, Liu X, Bao M, Hong Y, and Michalski G (2022) A diurnal story of $\Delta^{17}O$ NO_3^- in urban Nanjing and its implication for nitrate aerosol formation. *npj Climate and Atmospheric Science* 5(1). https://doi.org/10.1038/s41612-022-00273-3.

Zhao Y, Zhang YL, and Sun R (2021) The mass-independent oxygen isotopic composition in sulfate aerosol -a useful tool to identify sulfate formation: A review. *Atmospheric Research* 253. https://doi.org/10.1016/j.atmosres.2020.105447.

Zhou T, Jiang Z, Zhou JC, Zhao WX, Wu YC, Yu H, Li WK, Zhang ZY, Su GM, Ma TM, and Geng L (2022) Fast and efficient atmospheric NO_2 collection for isotopic analysis by a 3D-printed denuder system. *Analytical Chemistry*. https://doi.org/10.1021/acs.analchem.2c02839.

Zong Z, Shi XL, Sun ZY, Tian CG, Li J, Fang YT, Gao HW, and Zhang G (2022) Nitrogen isotopic composition of NO_x from residential biomass burning and coal combustion in North China. *Environmental Pollution* 304. https://doi.org/10.1016/j.envpol.2022.119238.